Doctoral Thesis

Functional role of the mesolimbic system in motor control

Suzuki, Michiaki

Doctor of Philosophy

Completion in March, 2018

Department of Physiological Sciences,

School of Life Science,

SOKENDAI

Table of contents

General introduction

It is believed that higher motivation boosts motor performance. For example, world records are often broken during prestigious competitions in sports. During such competitions athletes would get psyched up for obtaining fame, gold medal and/or money. For the patients with neuronal damage, motivation to engage in rehabilitative training would be also important for functional recovery. Alf Brodal, in his literature describing his subjective experience of recovery after stroke, mentioned that "mental energy" was closely coupled with contraction of his paretic muscles (Brodal, 1973). Furthermore, clinical studies suggest that improving depressive symptoms may accelerate functional recovery after neuronal damage (e.g. Chemerinski *et al.*, 2001; Saxena *et al.*, 2007). Thus, mental state might be a key issue for motor performance in healthy population, and furthermore, for functional recovery after neuronal damage in patients. However, the neural mechanism underlying such psychological effects on motor outputs or recovery is still unclear. Several recent studies have demonstrated that the reward-related information which induces incentive motivation modulates the activity of the primary motor cortex (M1) in humans (Pessiglione *et al*., 2007; Kapogiannis *et al*., 2008; Thabit *et al*., 2011;

Schmidt *et al*., 2012) and in non-human primates (Marsh *et al.*, 2015). These results imply that brain areas related to regulation of motivation may modulate the brain activity of motor-related areas, which would facilitate motor outputs.

The mesolimbic system consisting of the ventral tegmental area, the medial part of substantia nigra pars compacta in the ventral midbrain (VM) and the ventral striatum (VSt) are considered to process motivation for goal-directed behaviors (Salamone and Correa, 2012; Floresco, 2015). From neuroanatomical point of view, the VM has direct projection to the M1 (Gasper *et al*., 1992; Williams and Goldman-Rakic, 1998). However, whether this pathway effectively enhances the motor outputs from M1 or not remains unclear. To address this question, in the Part I of this thesis, I examined the hypothesis that the VM is involved in modulation of motor outputs from M1. To demonstrate this hypothesis, I investigated the polysynaptic anatomical connection from the VM to the spinal circuits controlling muscle activities using a retrograde transsynaptic tracer in monkeys. Furthermore, to understand the functional role of the oligosynapytic VM–spinal pathway, I investigated cortical and muscle responses induced by the VM stimulation.

The VSt, as another part of the mesolimbic system, is involved not only in processing motivation but also in exertion of physical effort (Aberman and Salamone, 1999; Schmidt *et al.*, 2012). A recent non-human primate study with the spinal cord injury (SCI) has revealed that the VSt up-regulates the M1 activity during early recovery stage after SCI and becomes more directly involved in the control of finger movements than before the injury (Sawada *et al.*, 2015). However, the causal contribution of the VSt to the functional recovery still remains unclear. Thus, in the Part II of this thesis, I hypothesized that the VSt might be more critical for the recovery of movements that demand higher physical efforts than less demanding movements. To address this question, I investigated the neural substrates underlying the control of highly demanding-dexterous movements, and less demanding movements in the intact state and after SCI, respectively, by measuring cerebral blood flow as an index of the brain activity with positron emission tomography. Furthermore, to clarify the causal role of the VSt in recovery of demanding dexterous finger movements such as precision grip, I investigated the effect of the permanent lesion of the VSt on motor recovery of dexterous and less dexterous finger movements after SCI.

Up to today, many scientists have clarified the mesolimbic function as a motivation/reward center. However, in this thesis, I demonstrated the functional role of the mesolimbic system in motor control, that is, the neural substrate bridging the mesolimbic system and the motor-related network. Together with previous findings and my results, I propose that the mesolimbic system might be a modulatory node which can regulate motivation and motor outputs simultaneously.

Part I

Title: Macaque ventral midbrain facilitates the output to forelimb muscles via the primary motor cortex

Abstract

Higher motivation boosts motor performance, but little is known about the neural substrate underlying such a psychological effect on motor output. Several recent studies in humans and non-human primates have revealed that activity of the primary motor cortex (M1) is modulated by incentive motivation to obtain reward. In the processing of motivational signals, the ventral midbrain (VM) is known to be an important brain area. Although the VM projects directly to the frontal cortical areas including the M1, it remains unknown whether the VM connects to the corticospinal pathway. Based on these lines of anatomical evidence, I hypothesized that the VM modulates the motor outputs from the M1. To investigate the existence of such a descending projection arising from the VM, rabies virus that permits retrograde transsynaptic transport was injected into the cervical enlargement of the spinal cord in macaque monkeys. I found the oligosynaptic projections from the VM, such as the ventral tegmental area, the substania nigra and the retrorubral field, to the spinal cord. To explore the functional significance of the oligosynaptic VM–spinal pathway as a modulator of the motor outputs, electrical stimulation was delivered to the VM and evoked responses were

recorded from the frontal cortical areas of the ipsilateral hemisphere and from upper limb muscles on the contralateral side to the stimulation sites under sedation. The VM stimulation induced field responses in the frontal cortical areas including the M1. Furthermore, evoked responses were also observed in upper limb muscles with a few milliseconds delay after the M1 response. Moreover, these muscle responses were diminished during the reversible inactivation of M1. The present study is the first report demonstrating the existence of the VM–M1–spinal pathway in non-human primates. This VM–M1–spinal pathway might be a candidate for the neural substrate underlying motivational control of motor outputs.

Abbreviations

LPFC, lateral prefrontal cortex

M1, primary motor cortex

OFC, orbitofrontal cortex

PM, premotor area

RRF, retrorubral field

SN, substantia nigra

VM, ventral midbrain

VTA, ventral tegmental area

Introduction

It is empirically believed that higher motivation boosts motor performance especially in prestigious competitions in sports. Several human studies have demonstrated that the incentive motivation instigated by monetary reward modulates the activity of the primary motor cortex (M1) (Pessiglione *et al*., 2007; Kapogiannis *et al*., 2008; Thabit *et al*., 2011; Schmidt *et al*., 2012). A recent study in non-human primates has demonstrated that the neuronal activity of the M1 during reaching movements is modulated by reward expectation (Marsh *et al.*, 2015). Thus, the M1 activity could be under control of incentive motivation. Reward/motivation-related activities are generally considered to be associated with activation of the ventral midbrain (VM), such as the ventral tegmental area (VTA) and substantia nigra (SN) pars compacta (Schultz *et al*., 1997, 1998; Matsumoto and Hikosaka, 2009). It has been repeatedly reported that the VM containing the VTA, SN and retrorubral field (RRF) has widespread direct projections to the frontal cortical areas including the M1 in non-human primates (Lewis *at al.*, 1987; Gasper *et al*., 1992; Williams and Goldman-Rakic, 1998) and also in rodents (Descarries *et al*., 1987; Hosp *et al*., 2011). Thus, the VM might exert an impact on motor behavior through

modulating the M1 activity. However, despite the evidence for the anatomical linkage from the VM to the M1, whether and how such a projection is effective to modulate the motor outputs remains elusive.

In the present study, I hypothesized that the VM might be a modulatory source of motor outputs. To address this issue, I first investigated the existence of multisynaptic projections from the VM to the spinal cord by injecting rabies virus that allows retrograde transsynaptic transport into the cervical enlargement. Secondary, to explore the functional significance of the identified VM–spinal pathway in modulating the motor output, the evoked responses by the electrical stimulation of the VM were recorded simultaneously from the frontal cortical areas including the M1 of the ipsilateral hemisphere and from multiple upper limb muscles on the contralateral side to the stimulation sites. Finally, to elucidate the causal contribution of the M1 to the muscle responses induced by the VM stimulation, I compared evoked muscle responses before and during the M1 inactivation. The overall results demonstrated the existence of the VM–M1–spinal pathway which can facilitate the output to forelimb muscles. This oligosynaptic pathway might constitute a neural substrate underlying motivational control of motor behavior.

Methods

Subjects

Five monkeys were used in the present study. I performed two kinds of experiments, the neuroanatomical and electrophysiological experiments. Two adult macaque monkeys (*Macaca mulatta*; Monkey F, female, 5.0 kg; Monkey L, female, 5.0 kg) were used for the neuroanatomical experiments. Three adult macaque monkeys (*Macaca mulatta*; Monkey T, male, 8.0 kg, *Macaca fuscata*; Monkey D, female, 5.5 kg; Monkey Y, female, 6.5kg) were used for a series of electrophysiological experiments.

Part 1. Neuroanatomical experiments

Subjects

Monkey F and Monkey L were used for the anatomical experiments. The experimental protocol was approved by the Animal Welfare and Animal Care Committee of the Primate Research Institute, Kyoto University (Approved No: 2015-050), and all experiments were conducted in accordance with the Guideline for the Care and Use of Animals of the Primate Research Institute, Kyoto University. Experiments involving the

rabies virus were performed in a special primate laboratory (biosafety level 2) designated for in vivo infectious experiments that had been installed at the Primate Research Institute, Kyoto University. Throughout the experiments, the monkeys were housed in individual cages that were installed inside a special biosafety cabinet.

Rabies virus

The challenge-virus-standard (CVS-11) strain of rabies virus was used to trace the multisynaptic projection from the VM to the spinal cord. The virus was originally obtained from the Centers for Disease Control and Prevention (Atlanta, GA, USA) and was donated by Dr. Satoshi Inoue (The National Institute of Infectious Diseases, Tokyo, Japan). The viral batch used in the present study was the same as in the previous study (Ishida *et al*., 2016). The titer of a viral suspension was 1.0×10^8 focus-forming units (FFU)/ml. According to the previous studies using rabies virus as retrograde transneuronal tracer (Kelly and Strick, 2003, 2004; Miyachi *et al*., 2005; Ishida *et al*., 2016), they concluded that it takes about 2 days for first-order neurons labeling and one additional day per synapse for subsequent transneuronal labeling following the cortical

injection of rabies virus. In the present study, rabies virus was injected into the spinal cord at the cervical level. It would take longer than 2 days to label first-order neurons in supraspinal areas (e.g. the M1) because distance from the spinal cord to the M1 is longer than cortico-cortical projections. Thus, the survival time in the present study was set at 3.5 or 3.75 days.

Surgery for viral injections

The monkeys were sedated with a combination of ketamine [10 mg/kg, intramuscular injection (i.m.)], and then anesthetized with sodium pentobarbital [20 mg/kg, intravenous injection (i.v.)]. All surgical procedures were performed using sterile technique. The skin and axial muscles were dissected at the level of the C3 to T2 vertebrae. Subsequently, laminectomy was performed to expose the cervical segments of the spinal cord. With the dura open, dorsal root entry zones were used to identify segmental levels. Thirteen penetrations spaced 2 mm apart were made rostrocaudally from C6 to T1 spinal segment. Small amounts of the virus were injected at different two depths along each track (0.5-0.6µl x 2 site per track, 13 tracks) through a 10 µl Hamilton microsyringe. The

syringe needle was tilted and entered the spinal cord at an angle. The angle and depth of the syringe required to reach the intermediate zone and ventral horn of the spinal cord were adjusted for each segment. A total of 13 (Monkey F) or 15.6 µl (Monkey L) of the viral suspension was injected into the spinal cord. After all injections were completed, muscle and skin were incised. Survival time for virus was set at 3.5 (Monkey F) or 3.75 days (Monkey L).

Histological procedures

With survival periods of 3.5 or 3.75 days after viral injection, the monkeys were deeply anesthetized with an overdose of sodium pentobarbital (50 mg/kg, i.v.) and transcardially perfused with 0.1 M phosphate-buffered saline (PBS), followed by 10% formalin dissolved in 0.1 M phosphate buffer (PB). The fixed brains were removed from the skull, postfixed in the same fresh fixative overnight at 4°C, and equilibrated with 30% sucrose in 0.1 M PBS at 4°C. Coronal sections were then cut serially at 50-µm thickness on a freezing microtome. Every tenth section was mounted onto gelatin-coated glass slides and Nissl-stained with 1% Cresyl violet. The remaining series of the sections 500

μm apart were processed for immunohistochemistry.

For immunoperoxidase staining for rabies virus, the sections were pretreated with 0.3% H_2O_2 for 30 min, washed three times in 0.1 M PBS, and immersed in 1% skim milk for 1 hr. Subsequently, the sections were incubated for 2 days at 4°C with rabbit anti-rabies virus antibody (donated by Dr. S. Inoue) in 0.1 M PBS containing 2% normal donkey serum and 0.1% Triton X-100. The sections were then incubated with biotinylated donkey anti-rabbit IgG antibody (1:1,000 dilution; Jackson laboratories, USA) in the same fresh medium for 2 hr at room temperature, followed by the avidin-biotin-peroxidase complex kit (ABC Elite; 1:200 dilution; Vector laboratories, USA) in 0.1 M PBS for 2 hr at room temperature. To visualize the antigen, the sections were reacted for 10-20 min in 0.05 M Tris-HCl buffer (pH 7.6) containing 0.04% diaminobenzine tetrahydrochloride (Wako, Japan), 0.04% $NiCl_2$, and 0.002% H_2O_2. These sections were counterstained with 0.5% Neutral red, mounted onto gelatin-coated glass slides, dehydrated, and then coverslipped.

Data analyses for labeled neurons

Neuronal labeling was plotted with Neurolucida (MicroBrightField, Inc., Williston, USA) on tracing of equidistant coronal sections (500 μm) through the VM. To display labeled neurons in the VM and the M1 on the contralateral to the injection side, photomicrographs were captured.

Part 2. Electrophysiological experiments

Subjects

To clarify the functional connectivity between the VM and muscles, I performed two kinds of electrophysiological experiments. One was recording cortical responses and muscle responses induced by the VM stimulation (Monkey D and T). Another was recording muscle responses before and during the M1 inactivation (Monkey D and Y). All three monkeys were chronically implanted a chamber for the VM stimulation and micro-wires into upper limb muscles for electromyogram (EMG) recording. Monkey D and Monkey T were also chronically implanted electrocorticogram (ECoG) arrays for recording cortical responses. In addition, Monkey D and Monkey Y were implanted an additional chamber for M1 inactivation study. A series of

electrophysiological experiments were approved by the Animal Experimental Committee of the National Institute of Natural Sciences (Approved No: 15A079), and was performed in accordance with the Institutional Guidelines for the Care and Use of Laboratory Animals.

Surgery

All surgeries described below were performed under general anesthesia initiated by ketamine (10 mg/kg, i.m.) plus xylazine (1 mg/kg, i.m.) and maintained with 1-1.5% isoflurane. Dexamethasone (0.825 mg/kg, i.m.), ampicillin (40 mg/kg, i.m.) and analgesic (0.25 mg/kg, i.m.) were administered after the surgery.

Chronic implant of ECoG arrays: To record cortical activities from frontal cortical areas including the lateral prefrontal cortex (LPFC), orbitofrontal cortex (OFC) and sensorimotor cortex such as the premotor area (PM) and M1, I used an ECoG electrode array. A platinum ECoG array (Unique Medical, Japan) was chronically implanted in two monkeys (Monkey D and T). The monkey's head was fixed in a stereotaxic apparatus. A median linear skin incision was performed on the head, and the skull was exposed over

the bilateral frontal and parietal cortices. The craniotomies were located around the arcuate sulcus and the central sulcus, respectively. The cortices around the arcuate sulcus and the central sulcus were exposed on left side. The ECoG array comprised of 21 channel (3 x 7 grid, inter-electrode distance 5 mm) electrodes was placed on the digit, hand and arm areas of the M1 and primary somatosensory cortex, PM and LPFC on left hemisphere. Another ECoG array comprised of 9 channels (3 x 3 grid, inter-electrode distance 3 mm) electrodes were placed on the left OFC. The electrodes had a diameter of 1 mm. Electrode locations were identified from anatomical views during the surgery. The reference and the ground electrodes were placed in the subdural space, facing the dura. The two openings of the skull were covered with acrylic resin.

Chronic implant of a chamber for VM stimulation: Magnetic resonance imaging (MRI) used to determine the precise geometry of the VM to allow accurate placement of microelectrode penetrations for VM stimulation. Scans were carried out under deep anesthesia which was introduced by ketamine (10 mg/kg, i.m.) plus xylazine (1 mg/kg, i.m.) and maintained with sodium pentobarbital (20 mg/kg, i.v.). T1-weighted images were collected with a 3 Tesla scanner (Allegra, Siemens, Germany). In three monkeys

(Monkey D, T and Y), surgery was performed to gain easy access for electrical stimulation of the VM. After the partial craniotomy, in which the center was located above the VM, a custom-made derlin chamber was attached to cover the craniotomy at an angle of 10° to the mid-sagittal plane (Monkey D and T) or without tilting (Monkey Y). Two titanium-steel tubes were mounted in parallel over the frontal and occipital lobes for fixation of the head. The chamber and stainless steel tubes were fixed to the screws with the acrylic resin.

Chronic implant of a chamber for M1 inactivation: An additional chamber was attached for M1 inactivation in Monkey D and Monkey Y. After the partial craniotomy, the cortex around the central sulcus was exposed unilaterally (right side for Monkey D and left side for Monkey Y), and a custom-made delrin chamber was attached to cover the craniotomy. Small titanium-steel screws were implanted in the skull as anchors. The skull and screws were completely covered with acrylic resin.

Chronic implant of microwires for EMG recordings: EMG activities of the upper limb muscles on contralateral side to the VM stimulation were recorded through chronically implanted pairs of multi-stranded stainless steel wires (Cooner Wire, Chatsworth, CA,

USA), which were subcutaneously tunneled to their target muscles. A connector (Samtec, Singapore) was anchored to the skull. EMGs were recorded from selected forelimb muscles. In Monkey T and Monkey D, EMGs on right forelimb were recorded from one shoulder muscle: pectoralis major (PEC), two elbow muscles: triceps brachii (TRI), biceps brachii (BB), five wrist muscles: extensor carpi radialis (ECR), extensor carpi ulnaris (ECU), flexor carpi radialis (FCR), extensor carpi ulnaris (FCU), palmaris longus (PL), four digit muscles: extensor digitorum communis (EDC), extensor digitorum 2,3 (ED23), flexor digitorum superficialis (FDS), flexor digitorum profondus (FDP), and one intrinsic hand muscles: first dorsal interosseous (FDI). In Monkey D, EMGs on left forelimb were recorded from one shoulder muscle: DEL, one elbow muscle: TRI, five wrist muscles: ECR, ECU, FCR, FCU, PL, EDC, two digit muscles: extensor digitorum 4, 5 (ED45), FDS and one intrinsic hand muscles: adductor pollicis (ADP). In Monkey Y, EMGs on right forelimb were recorded from one shoulder muscle: DEL, two elbow muscles: TRI, BB, five wrist muscles: ECR, ECU, FCR, FCU, PL, three digit muscles: EDC, ED45, FDS and one intrinsic hand muscles: FDI. The muscles in which the electrodes were implanted, were identified by stimulating through each electrode pair and

observing the evoked movements during the surgery.

Electrical stimulation to the VM

Before data collection, the monkeys were sedated with ketamine (10 mg/kg, i.m.) and atropine (0.5 ml, i.m.). Then, the monkeys were seated on a primate chair with their head fixed. Additional doses of ketamine were given as needed to eliminate spontaneous movements during the data recording sessions. Stimulation sites in the VM were stereotaxically determined based on the MRI image. Stimuli were delivered using bipolar concentric tungsten, platinum or stainless electrodes (impedance: 500-600 kΩ, Unique Medical, Japan). They were positioned in the recording chamber with an X-Y grid, guided through the cerebrum via a stainless steel cannula using an X-Y coordinate manipulator mounted on the head chamber. The electrode was inserted into the unilateral VM using a manual hydraulic microdrive (S Co., Ltd., Japan). Stimulus trains with current of 100, 300 or 500 μA were delivered to the target location more than 15 times through a constant-current stimulator. Only 300 μA was delivered to the VM for M1 inactivation study. Stimuli consisted of 3 biphasic pulses with 0.2 ms square-wave

duration at a frequency of 300 Hz. Stimulus trains were separated by more than 470 ms. To cover the target area globally, the stimulation was delivered antero-posteriorly or medio-laterally at every 1 mm. The electrode was advanced from the dorsal-to-ventral direction at every 0.5 or 1 mm step intervals and the process was repeated.

M1 inactivation

To determine the injection sites, the somatotopic maps were investigated with intracortical microstimulation (ICMS) under sedation with ketamine (10 mg/kg, i.m.). A tungsten microelectrode (1.1-1.5 MΩ at 1 kHz) was inserted perpendicularly to the cortical surface using a hydraulic micromanipulator. Regions in the precentral gyrus were mapped with ICMS. Each pulse had a positive phase followed by a negative phase, with each phase having a duration of 0.2 ms. Stimulus trains (currents of less than 50 μA at 333 Hz) were delivered through a constant-current stimulator. The number of pulses per train was 15. Each track was separated by 2 mm. Evoked movements of various body parts were carefully observed. The evoked movements detected by visual inspection were further monitored by direct muscle palpation.

A stainless steel microinjection needle (26 G) connected to a 10 μl Hamilton microsyringe (Hamilton Company, USA) via microtube was mounted on the same stereotaxic manipulator used for ICMS, so that the needle was inserted into the same track as the electrode for ICMS. Muscimol, a γ-aminobutyric acid type A ($GABA_A$) receptor agonist (5-6 sites, 1μl/site, 5 μg/μl, dissolved in 0.1 M PB, pH 7.4) was slowly injected by pressure at a rate of 0.2 μl/min. The depth chosen for muscimol injection had the lowest motor threshold. A total of 5 or 6 μl of muscimol solution was injected into the M1 digit, wrist and shoulder areas in Monkey D and into the M1 digit and wrist areas in Monkey Y, respectively. As a control condition, saline was injected at the same sites and the same volume as muscimol.

Data collection

Time stamps for the timing of the stimulation, ECoG signals from ipsilateral cortices to the stimulation side and/or EMG signals from contralateral side to the stimulation side were recorded simultaneously with a Cerebus™ data acquisition system (BLACKROCK MICROSYSTEMS, USA) at a sampling rate of 2,000 Hz. ECoG and/or

EMG signals were extracted using multi-channel amplifiers with a band-pass analogue filter (0.3 Hz high-pass and 7,500 Hz low-pass) and with band-pass digital filters in the Neuronal Signal Processor (0 Hz high-pass and 2,000 Hz low-pass for ECoG signals and 30 Hz high-pass and 1,000 Hz low-pass for EMG signals, respectively).

Data analyses

Stimulus-triggered averages of cortical responses and EMGs: The technique of the stimulus-triggered averages (StTAs) of ECoG and rectified EMG of all the recorded signals were constructed using custom-written software in Matlab 2012b (The MathWork, Natick, MA). Raw StTAs were aligned with the time of the first stimulus and included data from -100 to 200 ms around this time. To detrend the baseline activity from original StTAs trace, I subtracted the mean baseline activity (-100 to 0 ms) from the original StTAs trace. Then, the StTAs were normalized by standard deviation of the baseline for each signal, and expressed in multiples of the SD of the baseline (signal-to-noise ratio) (Cheney *et al*., 1991). The StTAs of ECoG responses were identified as having significant responses when the evoked response exceeded ± 2 SD of the baseline (-100 to 0 ms)

between 0 and 200 ms after stimulus onset. Each muscle was considered to have a significant activation when the magnitude of StTA of the rectified EMG response exceeded + 2 SD of the baseline and had a total duration ≥ 3 ms between 5 and 25 ms after stimulus onset.

Quantification of muscle responses: Onset and offset of the evoked muscle responses were defined as the initial point and final point in the first period during which the data points continuously exceeded + 2 SD, respectively. Data in which the onset was not able to identify because of stimulus artifacts were excluded. The mean percent increase (MPI) measured the average values between onset and offset of the feature minus the baseline mean, divided by the baseline mean (Fetz and Cheney, 1980). To confirm the effect of M1 inactivation on evoked muscle responses by VM stimulation, I compared MPI before and after microinjection of muscimol or saline (paired t-test, $P < 0.05$). In this analysis, I accepted data showing no significant change (paired t-test, $P < 0.05$) in MPI between the initial period of a session (stimulus counts: 1-250) and the last period (stimulus counts: 751-1000) in both conditions before and after microinjection. For accepted data, I compared the feature duration (> + 2 SD) before with after microinjection, and then I

adopted longer feature duration for MPI calculation.

Histological confirmation of stimulation sites

To identify stimulation sites, I marked the stimulus sites by electrocoagulation, which was made with rectangular constant current at 30 μA for 20 s through the stimulating electrode at the end of the experiment of all monkeys. During the electrocoagulation the monkeys were deeply anesthetized with an overdose of sodium pentobarbital (50 mg/kg, i.v.) and successively perfused transcardially with 0.1 M PBS (pH 7.3), followed by 4 % paraformaldehyde in 0.1 M PB (pH 7.3). The brain was removed from the bone immediately, and saturated with 10% sucrose in 0.1 M PB (pH 7.3), followed by 20% and 30% sucrose in 0.1 M PB (pH 7.3). The perfused brain was serially cut at 50-μm-thick coronal sections with a freezing microtome (MICROM HM450, WAKENYAKU CO., LTD., Japan), and one from every fifth section was mounted onto a gelatin-coated glass slide and Nissl-stained with 0.1% cresyl violet. The photomicrographs of the stimulation sites were captured, and then reconstructed. Electrical stimulation sites were estimated based on the location of coagulation in coronal

sections of the brain (Fig.3B and 4D). Cytoarchitectonic structures of the VM were identified according to the stereotaxic atlas (Paxinos *et al*., 2008).

Results

Retrogradely labeled neurons in the VM after rabies injections into spinal cord

To investigate the possible linkage of the transsynaptic VM–spinal pathway, two monkeys (Monkey F and Monkey L) received rabies injections into the cervical enlargement (C6–T1). The unilateral rabies injections were targeted around layer VII and IX where the spinal premotor interneurons (Perlmutter *et al.*, 1998) and motoneurons (Jenny and Inukai, 1983; Chiken *et al*, 2001) are distributed, respectively. In these cases, the monkeys were allowed to survive for 3.5 (Monkey F) or 3.75 days (Monkey L) post-injection. Fig.1A shows representative distribution of labeled neurons through the VM obtained from Monkey L. I found labeled neurons in the VM and red nucleus bilaterally. Labeled neurons in the VM were widely distributed throughout the entire rostrocaudal extent of the VM including all three of the mesencephalic dopamine (DA) cell groups, the VTA, SN and RRF. As illustrated in Fig.1A, the caudal part of the VM such as caudal SN and RRF contained larger number of labeled neurons than the rostral VM such as VTA and rostral SN. In addition, both contralateral and ipsilateral to the injection side

have labeled neurons. Photomicrograph of retrogradely labeled neurons in the SN or VTA were shown in Fig.1Bb and 1Bc, respectively. This tendency was commonly observed in Monkey F, although number of labeled neurons in the VM was smaller than that of Monkey L because of shorter survival time and less amount of injection volumes (13 μl for Monkey F vs 15.6 μl for Monkey L).

I then examined neuronal labeling in the motor-related areas including the M1. Cortico-spinal (CS) cells make monosynaptic connections with the spinal motor neurons and/or spinal interneurons, and these CS cells dominantly locate in layer V of the M1. Thus, the first-order neurons from the spinal cord are in layer V of the M1. The second-order neurons, neurons in layers III and VI of the M1, become infected after CS cells in layer V (Rathelot and Strick. 2006). As illustrated in Fig.1Cb and 1Cc, pyramidal neurons in layer V and in layer III of the contralateral M1 were labeled, respectively. I also confirmed the labeled neurons in layer III and V of the ipsilateral M1, which number was less than the contralateral M1. Furthermore, small number of layer V neurons in the contralateral pre-supplementary motor area (Pre-SMA) were labeled. The Pre-SMA has direct projections to the rostral PM and SMA (Luppino *et al.*, 1993) which have direct

projections to the spinal cord (He *et al.*, 1993). Furthermore, the Pre-SMA disynaptically projects to the M1 (Miyachi *et al.*, 2005) but not monosynaptically (Luppino *et al.*, 1993). Thus, labeled neurons in the Pre-SMA were likely to be second-order neurons via the PM and/or SMA or third-order neurons via the M1. These results indicate that the survival time in the present study was able to investigate maximally third-order neurons from the spinal cord. From these evidences, the present anatomical result demonstrated that the VM has oligosynaptic anatomical projections, presumably di- or trisynaptic connection to the cervical spinal motoneurons.

Cortical evoked responses by VM stimulation

To elucidate spatiotemporal dynamics of neuronal responses to the VM stimulation, I stimulated 31 sites (29 sites for 500 μA) in the VM in Monkey D and 5 sites in Monkey T and recorded cortical responses from frontal cortices. Fig.3B shows stimulation sites in Monkey D and Monkey T. All stimulation sites could evoke significant responses in the OFC, LPFC, PM and M1 at 100, 300 and 500 μA (Table.1). StTAs of ECoG signals were compiled for each stimulation site. An example of the StTAs

of cortical responses is shown in Fig.2A. Three pulses electrical stimulation of the VM evoked short-latency negative responses in the ECoG recordings in the OFC, LPFC, PM and M1 immediately after stimulus onset (~ 5 ms). Short-latency evoked responses in the PM and M1 were quite similar and the stimulus dependent responses lasted for ~100 ms after stimulus onset. Evoked responses in the LPFC and OFC have second and third negative peaks outlasting for ~200ms (Fig.2A and 2B). Majority of the stimulation sites in the VM showed fast negative-going responses in the PM and M1 at the latencies between 3 and 5 ms after onset of the VM stimulation, while minority of the stimulation sites showed positive-going responses at nearly 50 ms after the stimulus. Majority of the stimulation sites showed responses in the OFC at the latencies between 3 and 20 ms while in minor cases the latencies were between 20 and 30 ms as well as in the LPFC. In a few stimulation sites, faster negative-going responses within ~ 3 ms were found in the OFC and LPFC (Fig.2A and 2B). These results indicate that the VM has functional connectivity with frontal cortices including motor-related areas, and suggest that the VM could modulate cortical activities not only in prefrontal cortex (LPFC and OFC) but also in motor-related areas.

Evoked muscle responses by VM stimulation

Significant muscle responses were evoked in upper limb muscles by the VM stimulation at 300 μA in 17 out of 31 stimulation sites (54.8 %) in Monkey D and 2 out of 5 stimulation sites (40 %) in Monkey T, respectively. When the current intensity increased up to 500 μA, the number of effective sites increased. Stimulation with current of 100 μA was less effective to induce significant muscle responses. Percentage of effective stimulation sites decreased to 19.4 % (Monkey D) and 20 % (Monkey T), respectively (Table.1). An example of the StTAs of rectified EMGs is shown in Fig.3A. The VM stimulation induced responses in multiple muscles contralateral to the stimulation sites regardless proximal and distal muscles. Furthermore, some stimulation sites also induced leg movements (visual observation). The timing of the muscle responses followed the M1 responses (Fig.3A). Average and range of the onset latencies in all the recorded muscles from shoulder, elbow, wrist, digit and intrinsic hand muscles were shown in Table.2. Onset latencies were distributed mainly in the range of approximately 10 – 20 ms. Stimulation sites in the VM where electrical stimulation

induced muscle responses were scattered in the VM (Fig.3B) similar to the distribution of labeled neurons in the tanssynaptic tracing study (Fig.1A). Since the VM had the direct anatomical projection to the M1 (Gasper *et al*., 1992; Williams and Goldman-Rakic, 1998) and the VM stimulation evoked M1 responses, the M1 might contribute to these evoked muscle responses.

Effect of M1 inactivation on evoked muscle responses by VM stimulation

To clarify whether the M1 mediates the muscle responses evoked by the VM stimulation (Fig.4A-D), I performed focal inactivation of the M1 forelimb areas by microinjections of muscimol and compared evoked muscle responses before and during M1 inactivation. I performed ICMS mapping before the inactivation study to obtain a topographical map of the M1 for determination of the sites for inactivation. Muscimol was injected into the wrist and digit areas mainly with a total amount of 5-6 μl (Fig.4Aa and 4Ab). To minimize current spread to outside of the VM, stimulation with current of 300 μA was delivered to the VM in the M1 inactivation study. Evoked muscle responses by the VM stimulation were disrupted during M1 inactivation (Fig.4Ba). To quantify the

induced muscle responses, I calculated the MPI. MPI was substantially decreased during M1 inactivation compared with before the M1 inactivation (Fig.4Ca, $P = 0.017 < 0.05$). As a control condition, I injected saline into the same sites with the muscimol injection sites. Evoked muscle responses by the VM stimulation were not affected after saline injection (Fig.4Bb). There was no significant difference in MPI before and after saline injection (Fig.4Cb, $P = 0.12$). This result indicates that the M1 causally mediates the muscle responses evoked by the VM stimulation and suggests that the VM–spinal pathway is relayed by the M1 (Fig.5).

Discussion

The present study is the first report on the spatiotemporal dynamics of neural responses in the frontal cortices and muscle responses induced by electrical stimulation of the VM in non-human primates. The major findings of this study are, 1) the VM has the oligosynaptic projection to the spinal cord (Fig.1); 2) the VM stimulation evokes cortical responses in frontal cortices including the OFC, LPFC, PM and M1 (Fig.2) and induces muscle responses in multiple upper limb muscles (Fig.3); 3) these muscle responses are mediated by the M1 (Fig.4). These results demonstrated that the VM–M1–spinal pathway which could facilitate muscle activities via the M1 (Fig.5).

Fast cortical responses induced by VM stimulation

The result in the current study showed that the VM modulated the activity of frontal cortices. Majority of the stimulation sites in the VM showed fast negative-going responses in the PM and M1 at the latencies between 3 and 5 ms after onset of the VM stimulation. Majority of the stimulation sites in the VM showed responses in the OFC at the latencies between 3 and 20 ms as well as the LPFC (Fig.2A and 2B). This finding

demonstrated that the VM stimulation can modulate activities of limbic area and motor-related areas simultaneously. These brain areas showing evoked responses by the VM stimulation were consistent with brain imaging studies such as fMRI in monkeys (Arsenault *et al*., 2014) and optical imaging in rodents (Watanabe *et al*., 2009; Kunori *et al*., 2014). However, these imaging techniques have less information about the temporal dynamics of the neuronal activity than the electrophysiological recording. In this study, to understand more precise temporal dynamics in neuronal activity induced by the VM stimulation, I employed the electrophysiological recording. Since the fast responses were elicited within ~ 5 ms after onset of stimulation, they might include both orthodromic activation of the VM neurons, and antidromic activation of axons innervating the VM, which is necessary to be considered.

The VM, which contains both non-DA neurons and DA neurons, has direct projections to frontal cortical areas including the OFC, LPFC and M1 (Williams and Goldman-Rakic, 1998). Thus, it is possible that the VM stimulation can induce orthodromic activation of the VM neurons and its effects in the OFC, LPFC and M1. My result showed fast negative-going responses within ~ 5 ms latencies after onset of

stimulation (Fig.2A, 2B). However, DA is thought to act as a slow modulator of cortical neurotransmission. Thus, it is unlikely that DA released from the dopaminergic axon terminals in cortical areas originated from the VM DA neurons induced the fast cortical responses in my result. A recent electrophysiological study has demonstrated that fast cortical responses in the PFC induced by the VTA stimulation was blocked by a glutamate receptor antagonist, but not by a DA receptor antagonist and that the VTA lesion by 6-hydroxydopamine injection diminished the fast cortical response in the PFC (Lavin *et al.*, 2005), suggesting that the VTA-induced fast cortical responses were primarily caused by orthdromic activation of glutamatergic axons from the VM neurons. There is a small number of projection from the dorsolateral PFC and OFC to both the VTA and SN compacta in monkeys (Frankle *et al.*, 2006). In the present study, the LPFC and OFC showed fast responses within ~ 3 ms after stimulation in a few stimulation sites, which was not observed in the PM and M1. Together with previous reports, it is likely that fast responses in the M1 and PM dominantly reflect orthodromic activation of glutamatergic axons from VM neurons. In contrast, the short latency responses (~ 3 ms) in the PFC and OFC might include the antidromic activation of axons of LPFC/OFC neurons terminating

in the VM while fast responses in the LPFC and OFC at the latencies between 3 and 20 ms dominantly reflect orthodromic activation in the present study.

The pathways for muscle activation by VM stimulation

Muscle responses induced by the VM stimulation with current of 300 μA were observed from nearly half of stimulus sites in the VTA/SN/RRF (Table.1 and Fig.3B). Using retrograde transsynaptic tracer, I demonstrated that the VM has oligosynaptic anatomical projections to the spinal cord and labeled neurons in the VM were maximally third-order neurons from the spinal cord (see, Result). To the best of my knowledge, it has not been shown that an anatomical evidence confirming the direct projection from VM to spinal cord. My result that the M1 inactivation disrupted evoked-muscle responses (Fig.4Ba and 4Ca) indicates no or less direct projection from the VM to the spinal cord and the causal contribution of the M1 to evoked muscle responses by the VM stimulation. Thus, together with this result and previous findings of the direct VM–M1 pathway (Gasper et al., 1992; Williams and Goldman-Rakic, 1998), labeled neurons in the VM were potentially second- or third-order neurons via the M1. Thus, the present finding

demonstrated the existence of the VM–M1–spinal pathway.

Because the anatomical location of the VM is close to the red nucleus and the cerebral peduncle, there is a possibility that electrical stimulation spread to vicinity to descending motor pathways such as rubrospinal tract or pyramidal tract those pathways mono-syaptically connect to spinal motoneurons. The onset latencies of muscle responses evoked by the VM stimulation in the present study were distributed for a wide range (Table.2). Furthermore, the mean onset latency (Table.2) was longer than that of the muscle responses in shoulder, elbow, wrist, digit and intrinsic muscles induced by the red nucleus stimulation, 7.9 ms (Belhaj-saif *et al*., 1998) and by the M1 stimulation, 9.2 ms (Park *et al*., 2004). If currents spread to vicinity to descending pathways in the present study, evoked muscle response should largely remain even during M1 inactivation. My result showed that evoked muscle response diminished substantially during M1 inactivation (Fig.4Ba and 4Ca). Thus, it is unlikely that evoked muscle responses in the present study were not induced by the current spread to the rubrospinal tract or pyramidal tract.

I injected transsynaptic retrograde tracer into unilateral spinal cord, and found

labeled neurons in the bilateral VM. It has been shown that the unilateral M1 receives direct projections from the bilateral VTA/SN (Hosp *et al.*, 2011). In non-human primates, descending axons originated from the unilateral M1 terminates on spinal motor neurons and/or interneurons not only in the contralateral side but also in the ipsilateral side although ipsilateral corticospinal axons are minor compared with contralateral corticospinal axons (Bortoff and Strick, 1993; Lacroix S *et al.*, 2004; Rosenzweig *et al.*, 2009; Yoshino-Saito *et al.*, 2010). I also found labeled neurons in layer III and V of the ipsilateral M1. Thus, labeled neurons in the ipsilateral VM to the spinal injection side might relay the ipsilateral M1 to the spinal injection side. In addition, the number of labeled neurons was larger in the caudal VM (i.e. caudal SN/RRF) than the rostral VM (i.e. VTA/rostral SN). This might be attributed to the fact that the caudal SN and RRF contain larger number of neurons directly projecting to the M1 than the VTA and rostral SN (Williams and Goldman-Rakic, 1998).

Functional significance of VM-M1-spinal pathway

In reward prediction (Schultz *et al*., 1997, 1998) and processing motivation to

obtain reward (Matsumoto and Hikosaka, 2009), DA neurons in the midbrain are functionally important. In competitive sports, up-regulation of motivation is thought to be critical for enhancing performance. World records are often broken during prestigious competitions in sports. Tod *et al.* (2003) has suggested that psyching-up may enhance performance requiring force production such as strength, muscular endurance and power. During such competitions, athletes would psych themselves up to obtain reward such as fame, gold medal or money. Recent human studies (Pessiglione *et al*., 2007; Kapogiannis *et al*., 2008; Thabit *et al*., 2011; Schmidt *et al*., 2012) and a monkey study (Marsh *et al.*, 2015) have demonstrated that the reward information modulates the M1 activity. Thus, incentive motivation to obtain reward such as fame or money may be affect performance. My findings showed the short-latency responses in the frontal cortices such as motor-related areas and limbic area and muscles by the VM stimulation. In sports that crucially depend on maximum motor output, such as weightlifting, instantaneous muscle activations are required. The present result showing the facilitation of outputs to muscles via the VM–M1–spinal pathway might be a candidate for neural substrate underlying motivational control of motor outputs. Furthermore, in rehabilitation after neural damage,

it is generally thought that motivation to engage in rehabilitative training is important for functional recovery. It has been demonstrated that functional connectivity among the motivation-related brain areas and the M1 are strengthened during recovery after SCI (Nishimura *et al*., 2011). The ventral striatum, which has reciprocal connections with VM (Haber et al., 1990, 2000) up-regulates the activity of the M1 and is directly involved in the control of finger movements during early recovery stage after SCI. (Sawada et al., 2015) Thus, the VM–M1–spinal pathway may contribute to accelerate recovery after neural damage.

In conclusion, I demonstrated the existence of the VM–M1–spinal pathway with combination of anatomical, electrophysiological and pharmacological methods. I propose that the VM can boost motivation and motor outputs simultaneously. Further studies are needed to clarify the functional role of the VM–M1–spinal pathway during motor performance, motor leaning and rehabilitation for motor impairment.

Tables and legends

Table 1: Number of stimulation sites in VM inducing significant responses in frontal cortices and upper limb muscles.

Current of 100 μA

	OFC	LPFC	PM	M1	Muscle	# of tested
Monkey D	31 (100 %)	31 (100 %)	31 (100 %)	31 (100 %)	6 (19.4 %)	/ 31
Monkey T	5 (100 %)	5 (100 %)	5 (100 %)	5 (100 %)	1 (20 %)	/ 5

Current of 300 μA

	OFC	LPFC	PM	M1	Muscle	# of tested
Monkey D	31 (100 %)	31 (100 %)	31 (100 %)	31 (100 %)	17 (54.8 %)	/ 31
Monkey T	5 (100 %)	5 (100 %)	5 (100 %)	5 (100 %)	2 (40 %)	/ 5

Current of 500 μA

	OFC	LPFC	PM	M1	Muscle	# of tested
Monkey D	29 (100 %)	29 (100 %)	29 (100 %)	29 (100 %)	24 (82.8 %)	/ 29
Monkey T	5 (100 %)	5 (100 %)	5 (100 %)	5 (100 %)	3(60 %)	/ 5

"# of tested" indicates the total number of stimulation sites in the VM of each monkey. Number of and percentage of stimulation sites which induced significant responses in OFC, LPFC, PM, M1 and upper limb muscles are shown, respectively.

Table 2: Latency of muscle responses by VM stimulation.

Current of 100 μA

Joint	Onset Latency (ms)	Onset Latency Range (ms)	N
Shoulder	8.8 ± 1.7	5.5 ~ 10.5	3
Elbow	11.9 ± 2.3	8.0 ~ 18.0	4
Wrist	15.2 ± 1.6	12.5 ~ 18.0	3
Digit	11.3 ± 0.8	9.0 ~ 13.0	5
Intrinsic	—	—	0

Current of 300 μA

Joint	Onset Latency (ms)	Onset Latency Range (ms)	N
Shoulder	16.6 ± 2.1	11.0 ~ 25.0	7
Elbow	14.4 ± 1.2	8.5 ~ 19.0	9
Wrist	12.7 ± 0.6	9.0 ~ 19.0	23
Digit	13.7 ± 0.9	6.5 ~ 20.5	21
Intrinsic	18.2 ± 1.4	14.0 ~ 22.5	5

Current of 500 μA

Joint	Onset Latency (ms)	Onset Latency Range (ms)	N
Shoulder	13.0	—	1
Elbow	13.1 ± 0.8	8.5 ~ 21.0	19
Wrist	12.1 ± 0.4	9.0 ~ 23.5	59
Digit	12.9 ± 0.47	9 ~ 21.5	55
Intrinsic	14.8 ± 0.6	12.0 ~ 19.0	12

* Shoulder, PEC; Elbow, BB and TRI; Wrist, ECR, ECU, FCR, FCU and PL; Digit, EDC, ED23, FDS and FDP; Intrinsic, FDI.

Values are mean ± standard error of the mean (SEM). “N” indicates the number of

muscles showing significant activation in response to the VM stimulation. Muscles at each joint are indicated below the table. Data were obtained from right forelimb muscles of Monkey D and Monkey T.

Figures and legends

Figure 1

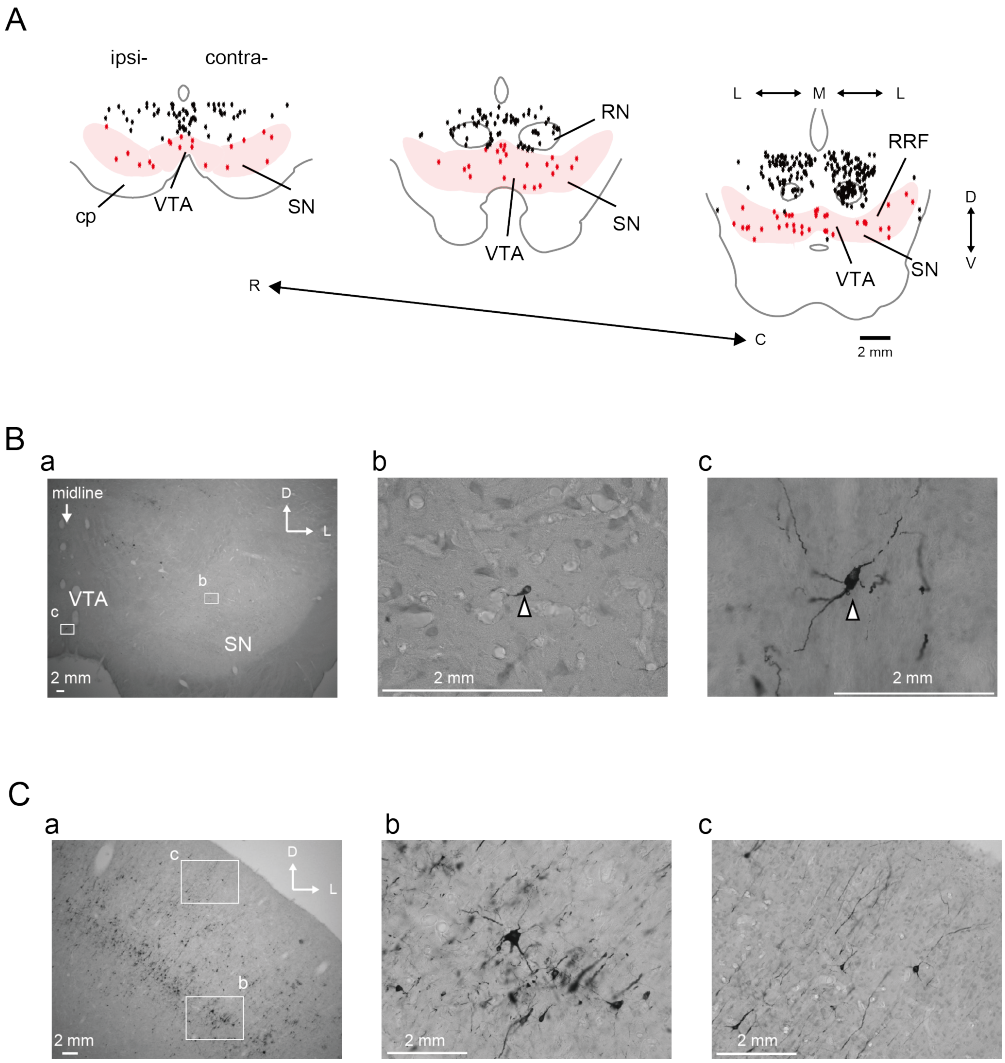

Figure 1: Oligosynaptic connection from the VM to the spinal cord. (**A**): Three representative coronal sections through the VM in Monkey L are arranged rostrocaudally. The areas of the VM are shown by shaded red color. Red dots indicate labeled neurons inside the VM. Black dots indicate labeled neurons outside the VM. Abbreviations: C,

caudal; D, dorsal; L, lateral; M, medial; R, rostral; V, ventral; ipsi-, ipsilateral side to the injection side; contra-, contralateral side to the injection side. (**B**): (a) Photomicrograph of the coronal section including the SN and VTA. (b, c) Higher magnification views of labeled neurons in the SN and the VTA, respectively. Magnification areas correspond to boxed-areas in (a). (**C**): (a) Photomicrograph of the coronal section including contralateral M1 to the injected side. (b, c) Higher magnification view of (b) layer V and (c) layer II/III.

Figure 2

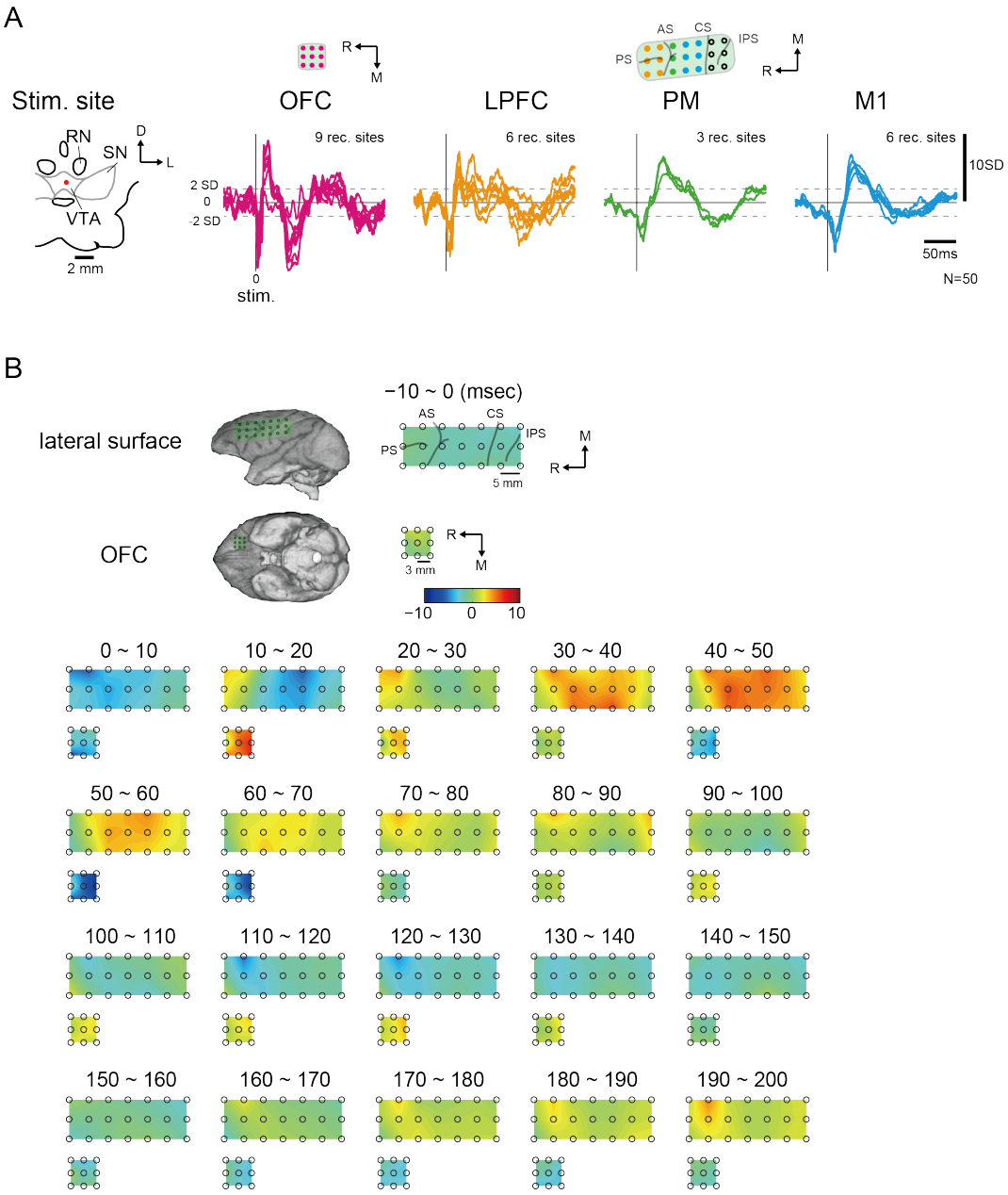

Figure 2: Cortical responses evoked by VM stimulation. (**A**): An example of StTAs of ECoG signals from the OFC, LPFC, PM and M1 (current intensity, 300 μA). Superimposed wave forms of the channels in each cortical area are shown in each panel.

The number of trigger events is indicated by ‘N’. Black vertical lines indicate stimulus onset and all signals aligned on this onset. Horizontal dashed lines indicate ± 2 SD lines based on the baseline activity (-100 ~ 0 ms). Vertical axis indicates signal-to-noise ratio. Stimulation site was indicated on the left side. Data were obtained from Monkey D. Abbreviations: M, medial; R, rostral; PS, principal sulcus; AS, arcuate sulcus; CS, central sulcus; IPS, intraparietal sulcus. (**B**): Time-dependent magnitude changes of cortical responses. Maps were expressed by mean magnitudes for 10 ms in individual channel. Red and blue colors indicate positive and negative values in signal-to-noise ratio, respectively. Dots on the map indicate electrode locations.

Figure 3

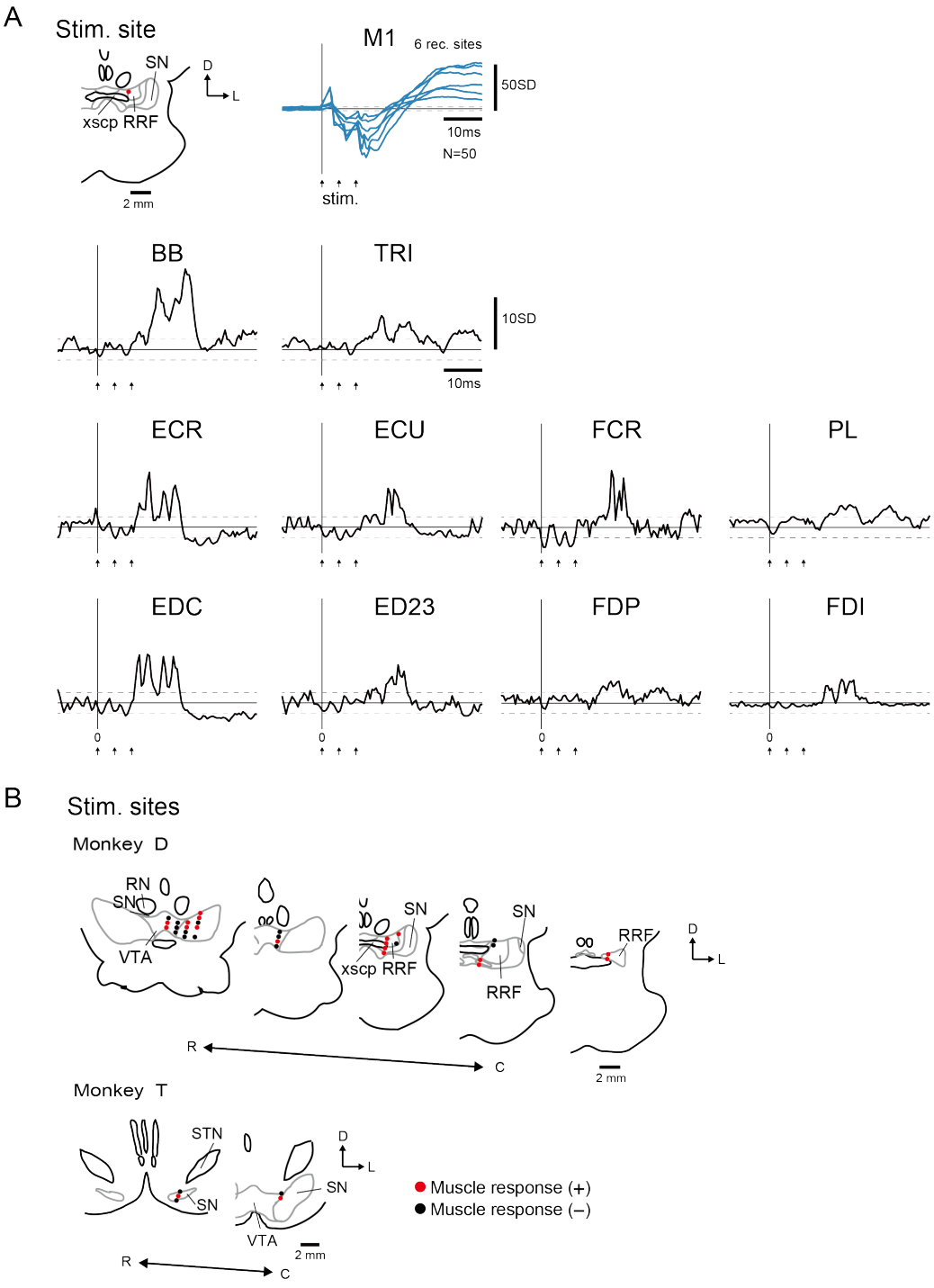

Figure 3: Responses in M1 and muscles evoked by VM stimulation. (**A**): An example of StTAs of ECoG signals in the M1 and StTAs obtained from rectified EMGs from 10

muscles (current intensity, 300 μA). Stimulation site was indicated on the upper left panel. Arrows indicate the timing of stimulus three pulses. Other legends are the same as in Fig.2A. Data were obtained from Monkey D. (**B**): Stimulation sites reconstructed from histological coronal sections in two monkeys. Outline of the VM was indicated by gray color. Red circles indicate stimulation sites which induced muscle responses with current of 300 μA. Black circles indicate stimulation sites which induced no muscle response with current of 300 μA. Abbreviations: D, dorsal; L, lateral; R, rostral; C, caudal; RN, red nucleus; xscp, decussation of the superior cerebellar peduncle.

Figure 4

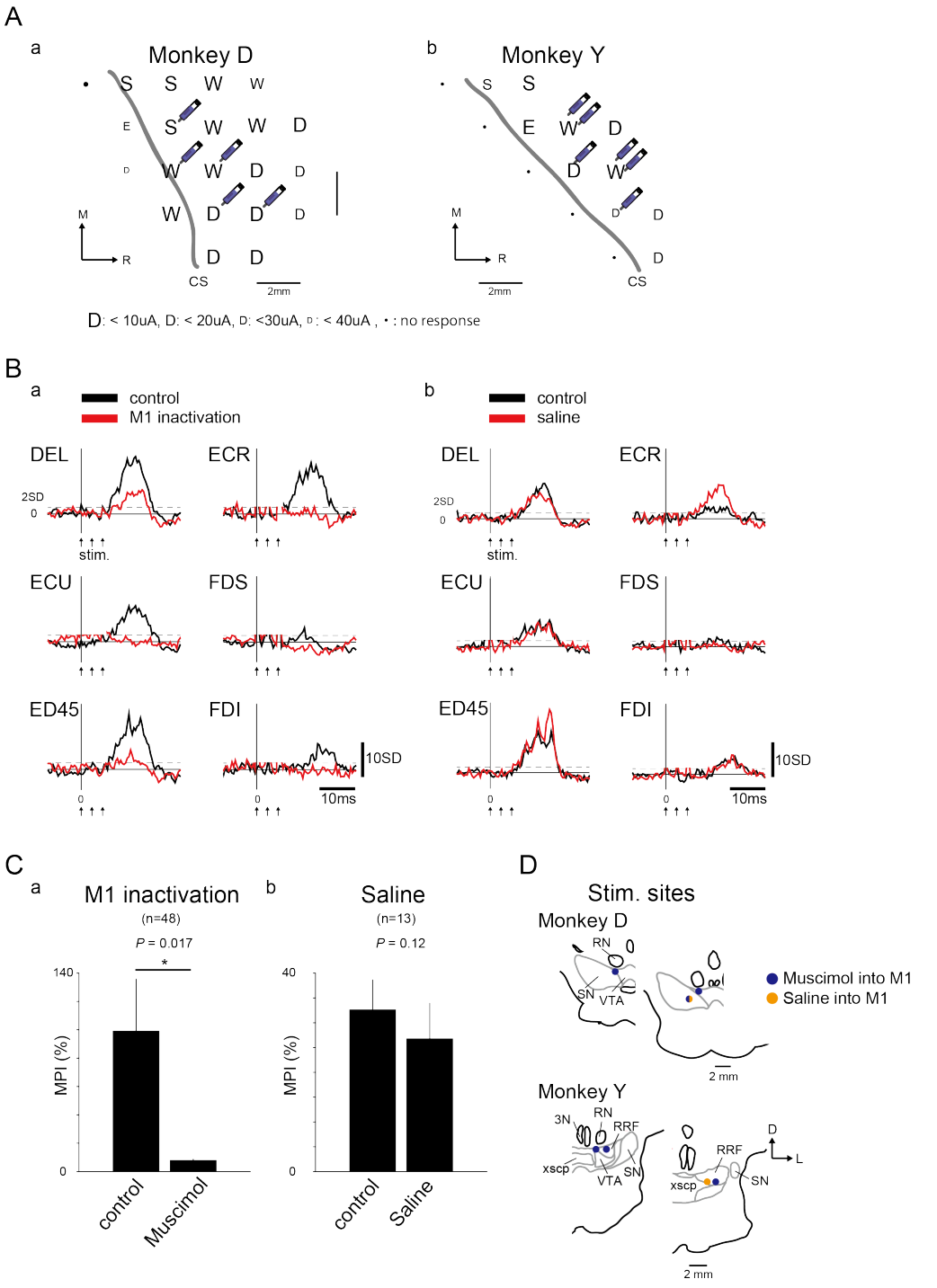

Figure 4: The effect of M1 inactivation on muscle responses evoked by VM stimulation. (**A**): Somatotopic map revealed by ICMS in (a) Monkey D and (b) Monkey

Y. Each electrode penetration is represented with a character indicating the body territory activated at threshold: D, digit; W, wrist; E, elbow; S, shoulder. The size of characters indicates the threshold for induction of movements (inset). The sites and volumes of muscimol injection are shown by syringes (1 μl/syringe). (**B**): Representative examples of StTAs obtained from rectified EMGs from 6 muscles (current intensity, 300 μA). Black and red traces indicate before injection either muscimol or saline into the M1 (control), and after those injections (M1 inactivation or saline), respectively. (a) Effect of M1 inactivation. (b) Effect of saline injection. (**C**): The effect of the M1 inactivation on MPI of muscles. (a) M1 inactivation, (b) Saline injection into the M1. Data obtained from two monkeys (Monkey D and Y) were combined. For statistical analysis, paired t-test was performed. Error bars indicate SEM. *, $P < 0.05$. (**D**): Stimulation sites reconstructed from histological coronal sections in Monkey D and Monkey Y. Outline of the VM was indicated by gray color. Purple circles indicate stimulation sites for the M1 inactivation. Orange circles indicate stimulation sites for saline injection into the M1. Abbreviations: D, dorsal; L, lateral; R, rostral; C, caudal; RN, red nucleus; xscp, decussation of the superior cerebellar peduncle; 3N, nucleus of oculomotor nerve.

Figure 5

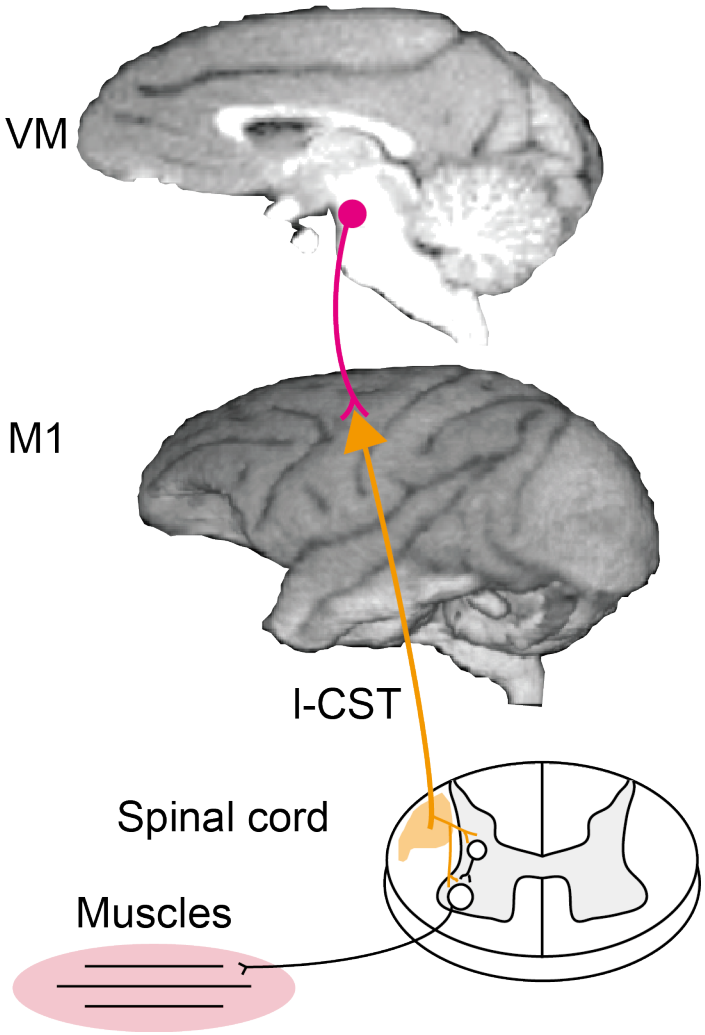

Figure 5: Proposed pathway bridging the VM and corticospinal tract. The VM oligosynaptically innervates the spinal motoneurons via the corticospinal neurons originating from the M1. Abbreviation: l-CST, lateral corticospinal tract.

Part II

Title: Causal role of the ventral striatum for the recovery of finger dexterity after spinal cord injury

Abstract

One of the most serious problems for individuals with motor paralysis after neuronal damage such as spinal cord injury (SCI) or stroke is deficit in dexterous finger movements such as precision grip. A great deal of effort and extensive rehabilitation are required to restore the finger dexterity. On the other hand, less dexterous coarse grip such as whole-finger grip is easier to maintain or to recover after the injury. The ventral striatum (VSt) is a key brain region mediating a variety of behaviors requiring motivation-driven effort, which is thought to promote functional recovery after neuronal injury while psychological problems such as depression impede recovery. Recently, it has been shown that the nucleus accumbens (NAc), a part of the VSt, up-regulates the neuronal activity of the primary motor cortex (M1) and becomes to directly control finger movements during early recovery stage after SCI in non-human primate. However, it is still obscure whether the VSt is essential for the functional recovery of finger dexterity. At first, by brain imaging study I investigated the difference in the neural substrate for the precision grip and for the whole-finger grip before and after SCI in monkeys. Results showed that during the precision grip task, more intense functional connectivity among the motor-

related networks including the contralesionl M1 (co-M1) emerged as compared to that during the whole-finger grip task. Furthermore, the functional connectivity between the co-M1 and the bilateral VSt emerged after SCI during the precision grip but not during the whole-finger grip. These results suggested that the VSt-motor-related network underlies the performance of precision grip during the recovery process. Secondary, I examined the effect of the bilateral VSt lesion on the recovery of finger movements after SCI. The VSt lesion showed no impairment of finger dexterity before SCI, while it impeded the recovery of precision grip but not coarse grip. Thus, these results demonstrate that the VSt is causally and specifically involved in the functional recovery of precision grip, and suggest that psychological and/or pharmacological approaches targeting the up-regulation of VSt can be possible treatments to promote functional recovery after neuronal damage.

Abbreviations

ACC, anterior cingulate cortex

co-, contralesional

CST, corticospinal tract

ip-, ipsilesional

M1v, ventral aspect of primary motor cortex

M1d, dorsal aspect of primary motor cortex

OFC, orbitofrontal cortex

PMv, ventral premotor area

PMd, dorsal premotor area

Pu, putamen

pre-SMA, pre-supplementary area

rCBF, regional cerebral blood flow

S1, primary somatosensory cortex

S2, secondary somatosensory cortex

SCI, spinal cord injury

VP, ventral pallidum

VSt, ventral striatum

Introduction

Neuronal damage such as spinal cord injury (SCI) and stroke leads to demanding situations represented by motor impairment. Individuals with motor impairment after neuronal damage are required to expend effort for voluntary movement. Brodal, in his literature describing his subjective experience of recovery after stroke, mentioned that "mental energy" was closely coupled with severity of his paretic muscles (Brodal, 1973). Depression is a common psychological problem after neuronal damage, and it has been shown to impede the functional recovery (Chemerinski *et al.*, 2001; Saxena *et al.*, 2007). Therefore, motivation-driven effort might be a key issue for facilitating recovery process. However, the neuronal substrate underlying such psychological effects on functional recovery remains obscure.

It has been reported the ventral striatum (VSt) plays a critical role in motivation-driven effort to obtain reward in animals (Aberman and Salamone, 1999) and in humans (Pessiglione *et al.*, 2007; Schmidt *et al.*, 2009, 2012). Recent non-human primate studies with SCI made at the C4/5 segment to transect the lateral corticospinal tract (l-CST) showed that functional recovery of finger dexterity was associated with

increased activity of the VSt (Nishimura *et al.*, 2007a, 2011), and further showed reversible pharmacological inactivation of the nucleus accumbens (NAc) as a part of the VSt, diminished high-frequency oscillatory activity in the primary motor cortex (M1) during early recovery stage after SCI accompanied by a transient deficit of amelioration in finger dexterity obtained by rehabilitation (Sawada *et al.*, 2015). Although these previous studies demonstrated that VSt had a functional role in controlling dexterous finger movements after SCI, it remains unclear whether the VSt is causally involved in functional recovery of dexterous finger movements after SCI.

Dexterous finger movements (e.g., precision grip) are severely impaired immediately after CST lesion (Lawrence and Kuypers, 1968, Nishimura *et al.*, 2007a, 2009; Higo *et al*., 2009) while coarse finger movements such as whole-finger grip, in which all digits are used in concert, recover earlier than the precision grip or remain unaffected by the injury. Non-human primate studies using SCI model (Nishimura *et al.*, 2007a) or M1 lesion model (Murata *et al.*, 2008) monkeys showed changes in their grasping strategy from premature grasping to precision grip during progression of recovery. These observations imply that dexterous finger movements might be more

demanding and require higher effort than whole-finger grip.

According to the above-mentioned findings, the VSt is suggested to be more essential for the recovery of highly demanding movement such as precision grip than less demanding whole-finger grip. To clarify the critical involvement of the VSt in the recovery of highly demanding movements, I first compared the neural substrates underlying the control of precision grip and whole-finger grip before and after SCI, respectively, by imaging the movement-related brain activity by positron emission tomography (PET). Furthermore, to investigate the causal contribution of the VSt to the motor recovery after SCI, I made bilateral lesions of the VSt by ibotenic acid injection. My results demonstrated that emergence of the VSt-motor networks was associated with recovery of precision grip, and further demonstrated the causal role of the VSt in functional recovery of dexterous finger movements after SCI. The present study suggests a possible modulatory action of the VSt in the neuroplastic reorganization of functional connectivity in the motor-related networks required for recovery of dexterous finger movements.

Methods

Subjects

Nine macaque monkeys were used for the present study. Three monkeys (Monkey H; *Macaca fuscata*, Monkey K and TF; *Macaca mulatta*; body weight 6.5-8.1 kg) were used for the PET experiment. Three monkeys (Monkey Ju, Na, and Sh; *Macaca mulatta*; body weight 3.6-4.9 kg) were used for the VSt lesion experiment (VSt lesion group). Three monkeys (Monkey M, T and R; *Macaca fuscata*; body weight 5.2-7.1 kg) were used for the VSt sham lesion experiment (Control group). The experimental protocols followed the guideline set forth by the Ministry of Education, Culture, Sports, Science and Technology (MEXT) of Japan, and were approved by the animal experimental committee of the National Institutes of Natural Sciences, that of Central Research Laboratory in Hamamatsu Photonics and that of Amami Wild Animal Research Center Inc.

Treatments related to surgeries

All surgeries described below were performed with sufficient sterilization

under general anesthesia, starting with a combination of intramuscular injections (i.m.) of ketamine (10 mg/kg body weight) and xylazine (1 mg/kg, i.m.) and succeeded by intubation and isoflurane (1-1.5%) inhalation to maintain stable, deep anesthesia throughout the surgery. Ampicillin (40 mg/kg, i.m.) was injected as an anti-biotic drug before the surgery, and dexamethasone (0.825 mg/kg) and ketoprofen (0.4 mg/kg) were administered for reducing postoperative pain and inflammation after the surgery.

Spinal cord injury

Lateral corticospinal tract (l-CST) lesions were performed as described elsewhere (Sasaki *et al.*, 2004; Nishimura *et al.*, 2007a, 2009, 2011; Sawada *et al.*, 2015). Briefly, the l-CST was partially transected in all monkeys after behavioral data were obtained in the intact stage. Under the above-mentioned anesthesia, the border between the C4 and C5 segments (C4/C5) was exposed by laminectomy of the C3 and C4 vertebrae, and a transverse opening was made in the dura. The dorsal part of the lateral funiculus was transected from the dorsal root entry zone ventrally to the level of the horizontal strip lesion. The lesion was extended ventrally at the most lateral part of the

lateral funiculus. The skin and back muscles incisions were closed with nylon or silk sutures.

Part 1. PET experiment

A part of behavioral and PET data, data in the precision grip task and the control task, I used in the present study have been published in previous articles from my group (Nishimura *et al*., 2007a, b, 2011) though data were reanalyzed using a new version of SPM software (SPM8) with a renewed monkey MRI brain template. The PET data of the whole-finger grip task, which were newly included in this analysis, were not used in the previous articles (see detail below).

Subjects

Monkey H performed with the right hand and received the l-CST lesion on right side. Monkey K and TF performed with the left hand and received the l-CST lesion on left side. During the behavioral test and training, the other hand was restricted. After taking an anatomical image of the brain using MRI, an acrylic head holder, which was

used for fixation of the monkey's head on the monkey chair in the PET gantry during the scanning, was attached to the skull.

Behavioral test

To assess the finger dexterity, the monkeys were trained to reach, grasp and retrieve a small piece of sweet potato (about 5 × 5 × 5 mm^3) attached to a pin inserted through the bottom of a horizontal tube positioned in the midsagittal plane (Pin task; Fig.6B). In addition, the monkeys were also trained to perform the same movement sequence, retrieve a small piece of food through a narrow vertical slit, which guides the monkeys to perform a precision grip (Slit task; Fig.6C). Each training session consisted of ~100 trials. Each testing session consisted of 30 trials. The definition of the successful precision grip was grasping and retrieving a food morsel with the pads of the index finger and thumb (i.e. index finger-to-thumb opposition) without dropping it. The coarse grip was defined when the monkeys retrieved a food morsel without dropping it with other gripping strategies. For example, whole-finger grip by a clenched hand, in which all digits were used in concert, holding a morsel between the pad of the index finger and nail of the

thumb, holding a morsel between the lateral side of the index finger and the pad of the thumb, and raking a morsel with the index finger. The rates of the precision grip and the coarse grip were calculated as the number of successful trials divided by 30. A digital video camera (33 frames/s) was used to record the reach-retrieval sequences from a lateral view. Both behavioral test and training session were executed before and after SCI.

Behavioral tasks in the PET experiment

The monkeys were trained to sit on the monkey chair and to perform the precision grip task, reaching, grasping and retrieving a small piece of food morsel through a narrow vertical slit using the pads of index finger and thumb (Fig.7A left, the same task with Fig.6C), with a constant interval (once per 5s) with the affected hand by SCI in both the training room and the PET scanner. In addition, they were trained to perform the whole-finger grip task, in which they were required to reach, grasp and retrieve an acrylic cylinder by a whole-finger grasping (Fig.7B left). A small piece of food was attached to the rear side of the cylinder. In both tasks, after grasping the monkey ate the piece of food. Furthermore, they were trained to the control task, in which the food morsel stuck at the

tip of the rod attached to a long tube was given to their mouth under restriction of both arms with the same pace as the reach and grasp task (see Nishimura *et al.*, 2007b).

PET scans

A series of PET scans for measurements of the regional cerebral blood flow (rCBF) as an index of the neuronal activity was conducted before the injury and during the early and late recovery stages (approximately 1 month and 3 months after SCI, respectively). The monkey was allowed to begin the behavioral task (20 trials) at about 10 s before the start of the PET scan with the delivery of a bolus of [^{15}O]H_2O (~300 MBq in 1.5 ml followed by 1.0 ml of saline) via a cannula inserted into the sural vein. The sessions of the precision grip task, the whole-finger grip task and the control task were randomly mixed. During the scan, the monkeys performed a series of reach-grasp-retrieve-eat movements every 5 s. In addition, PET data were collected for 80 s (one 40 s frame followed by four 10 s frames). Video recording of the scanning session was performed, and if the monkey did not start reaching within 500 ms after presentation of the food or did not move the hand directly to the food piece, the data was excluded from

analysis. The PET scans were performed when each monkey reached similar performance level, which was determined by the recovery level of the precision grip in the slit task (Fig.6Ca, see also Nishimura *et al.*, 2007a). The rate of precision grip was approximately 80 and 100 %, about 1 and 3 months after SCI, respectively. In Monkey H, PET scans were conducted between post-SCI Day 15 to 29 and between post-SCI Day 90 to 112. In Monkey K, PET scans were conducted between post-SCI Day 22 to 41 and between post-SCI Day 92 to 115. In Monkey TF, PET scans were conducted between post-SCI Day 36 to 64 and between post-SCI Day 106 to 122. Twenty-four scans were conducted on monkey H and K for all the three tasks for intact stage and 48 scans for recovery stages. Twenty-seven scans were conducted on monkey TF for intact stage and 55 scans for recovery stages.

Data Analysis for PET

Reconstructed brain images (voxel size, 1.2x1.2x3.6 mm), which were scalped and smoothed with a 4.0 mm FWHM isotropic kernel, were processed using statistical analysis of the parametric mapping (SPM8) software. PET images obtained from the scan

sessions that satisfied the behavioral criteria were summated for their first 60 s epochs, and were used for statistical analysis. The significant foci of inter-subject data were assessed using the analysis of covariance (ANCOVA) with global normalization. For the inter-subject analysis, brain shapes of individual [^{15}O]H_2O-PET images were morphologically normalized to a pseudo-brain template [^{18}F]FDG-PET image (voxel size, 0.5x0.5x0.5 mm), which was adjusted to the standard MRI template, originally created by 20 brain MRIs of young adult male macaque monkeys, using the product of transformation matrices: individual mean [^{15}O]H_2O-PET image to template [^{18}F]FDG-PET image. In order to localize the activity that reflected functional recovery, I defined the contrast as (precision grip/whole-finger grip task at the recovery stage - control task at the recovery stage) - (precision grip/whole-finger grip task at the intact stage - control task at the intact stage). This definition examines the main effect of the functional recovery of precision grip or whole-hand grip. The statistical threshold was set at $P <$ 0.01, uncorrected ($t > 2.33$). Any region that consisted of less than 250-clustered voxels was not considered a significant signal because of the limitation of spatial resolution. To determine the anatomical localization of activated foci, the SPM{t} PET images were

precisely co-registered to the template MRI.

For functional connectivity analysis, voxels of interest (VOI) for the M1 and VSt on the contralesional hemisphere (co-M1, co-VSt), which included the activated foci revealed by SPM analysis, were determined by the results of the main effect of the functional recovery of the precision grip (Fig.9A and Fig.11A). The regions where rCBF values were correlated with those of the co-M1 or co-VSt during the precision grip task or the whole-hand grip task were also determined by SPM analysis. The statistical threshold was set at $P < 0.01$, uncorrected ($t > 2.38$ for the intact, $t > 2.35$ for the recovery stage).

Part 2. VSt lesion experiment

Subjects

Monkey Ju, Na, and Sh received the bilateral VSt lesion (VSt lesion group). Monkey M, T, and R received the bilateral VSt sham lesion (Control group). All the six monkeys performed with the left hand and received the l-CST lesion on the left side. During the behavioral test and training, the other hand was restricted. The data from the

three monkeys of the control group were obtained from the previous study by my group (Sawada *et al.*, 2015).

Behavioral test

As described above, to assess the ability to control the dexterous finger movements, all the six monkeys were intensively trained to reach, grasp and retrieve a small piece of sweet potato through a narrow vertical slit using both the index finger and thumb (Slit task; Fig.14A) in their home cage (VSt lesion group) or on the monkey chair (control group). The definition of the precision grip and the coarse grip were described above. Each training session consisted of ~100 trials. Each testing session consisted of 30 trials. Video recording system and analysis procedures were also described above. Both behavioral test and training sessions were performed before and after the bilateral VSt lesion or sham lesion both before and after SCI (Fig.14B).

Bilateral VSt lesion

To define the location of the VSt I performed craniotomy and identified the

rostral arcuate sulcus spur in each hemisphere as a reference surface position. Ibotenic acid [15 μg/μl, dissolved in 0.1 M phosphate-buffered saline (PBS), pH 7.4] was injected to destroy neurons in the VSt, whose injection site was determined by stereotaxic coordinates according to the atlas by Paxinos (Paxinos *et al*, 2009). Multiple injections by a 10-μl Hamilton syringe (Hamilton Company, Reno, Nevada, USA) were performed to make the lesion of the whole VSt, with five tracks separated by 2 mm each other. In each track, injections were made at one or two separated sites by 2 mm in depth. Ibotenic acid was injected at a rate of 0.2 μl/min (9 sites/hemisphere, 1 μl/site).

As a sham lesion of the VSt, muscimol, a γ-aminobutyric acid type A ($GABA_A$) receptor agonist (5 μg/μl, dissolved in 0.1 M PBS, pH 7.4), was injected into bilateral VSt of the monkeys in the control group before SCI. A custom-made chamber was attached to cover the craniotomy, in which the center was located above the VSt. To make the sham lesion of bilateral VSt, Hamilton syringe needles for muscimol injection were inserted into the VSt (8 sites/hemisphere, 1 μl/site) as described in the previous paper (Sawada *et al.*, 2015).

Histological confirmation of the lesion extent

At the end of all these experiments, the monkeys were deeply anesthetized with an overdose of sodium pentobarbital (50-75 mg/kg, i.v.) and perfused transcardially with 0.1 M PBS (pH 7.4), followed by 4% paraformaldehyde in 0.1 M phosphate buffer (pH 7.4). The spinal cord and brain were immediately removed and immersed successively in 10, 20 and 30% sucrose solution of 0.1 M PBS (pH 7.3). Then, they were cut serially into 50-μm-thick coronal sections on a freezing microtome. All sections were processed for Nissl-staining with 1% cresyl violet.

Photomicrographs of the spinal cord lesion and the VSt lesion (only VSt lesion group) was captured. The extent of the VSt lesion in each subject was defined by the area of gliosis.

Results

Functional recovery after SCI in the PET experiment

Three monkeys (Monkey H, TF, and K) were tested on the PET experiments. Finger movements were impaired immediately after the SCI. The monkeys started rehabilitative training of food retrieval with the affected hand from the next day of SCI. In the pin task, in which the monkeys were retrieving the morsel from a tip, the coarse grip such as whole-finger grip by a clenched hand was observed immediately after SCI and disappeared in about 3 months (Fig.6Bb). On the other hand, the precision grip started to recover from postoperative day 10 and fully recovered in about 3 months (Fig.6Ba). Thus, grasping strategy changed from the coarse grip to the precision grip. In the slit task, in which the monkeys were retrieving the morsel through a narrow vertical slit, the monkeys showed full recovery of the precision grip within 1 month (Fig.6Ca). The coarse grip was rarely observed, even in early stage of recovery because the slit was guiding the monkeys to perform precision grip. (Fig.6Cb).

Increased activation in M1 and VSt during recovery after SCI

To clarify the difference in the brain activation between the precision grip task and the whole-finger grip task as a representative of coarse grip, I analyzed the rCBF during the precision grip task and during the whole-finger grip task before and after SCI. In both tasks, increased activity during the recovery stage was commonly found in the ventral aspect of the contralesional primary motor cortex (co-M1v) ($P < 0.01$, uncorrected, Fig.7Ab and 7Bb). Activity in the contralesional VSt (co-VSt) significantly increased during the precision grip task during the recovery stage relative to the intact stage, which was consistent with the previous study (Nishimura *et al.*, 2007a), but not during the whole-finger grip task ($P < 0.01$, uncorrected, Fig.7Aa and 7Ba). These results indicated that the M1v increased its activity to achieve the precision grip and the whole-finger grip after SCI. In addition, the VSt increased its activity for achieving the precision grip. Other sensorimotor-related areas such as the primary somatosensory cortex (S1) also showed increased activation in both tasks (Fig.8A, 8B and Table.3).

Functional connectivity between M1 and VSt emerged during the precision grip but not during the whole-finger grip after SCI

To clarify the neuroplastic change in the motor networks underlying the functional recovery, I performed correlation analysis which depicts functional connectivity of two brain regions. Functional connectivity between the co-M1v and VSt were investigated before and after SCI. VOI for the co-M1v were determined by the results of the main effect for the functional recovery of the precision grip (Fig.9A and Fig.10A). During the precision grip task, significant positive correlation with the co-M1v was found in the bilateral VSt in the recovery stage, but not in the intact stage ($P < 0.01$, uncorrected, Fig.9C and Table.4). In contrast, there was no significant correlation between the co-M1v and the VSt during the whole-finger grip task both before and after SCI (Fig.9D and Table.4). To confirm mutual connectivity between the M1v and the co-VSt, I used VOI in the co-VSt which were determined by the results of the main effect of the functional recovery of the precision grip (Fig.11A). Significant positive correlation with the co-VSt was found in the co-M1v and the ventral aspect of the ipsilesional M1 (ip-M1v) during the precision grip task in the recovery stage but not in the intact stage ($P < 0.01$, uncorrected, Fig.11Ce and 11De and Table.5). No significant positive correlation with the co-VSt was found in the co-M1v during the whole-finger grip task both in the

intact and recovery stage ($P < 0.01$, uncorrected, Fig.11Ee and 11Fe and Table.5). Thus, I found mutual functional connectivity between the co-M1v and co-VSt in the precision grip task, which was consistent with the previous study (Nishimura *et al.*, 2011), while not in the whole-finger grip task during the recovery stage.

VSt and M1 increased functional connectivity with other sensorimotor areas for the precision grip but not as much for the whole-finger grip after SCI

To understand the large scaled reorganization associated with functional recovery, I performed correlation analysis in the whole brain level. During recovery stage in the precision grip task, significant positive correlations with the co-M1v were found in the sensorimotor areas such as bilateral pre-supplementary motor area (pre-SMA), contralesional ventral premotor area (co-PMv), ip-M1v, ip-S1, bilateral putamen (Pu) and co-thalamus (Th) and the limbic areas such as contralesional orbitofrontal cortex (co-OFC) in addition to the bilateral VSt mentioned above. Such correlation was not observed preoperatively, but emerged during recovery (Fig.10C, 10D and Table.4).

Interestingly, these areas which showed positive correlations with the co-M1v

also showed positive correlations with the co-VSt. Fig.12A and Fig.13 showed brain regions revealing a significant correlation with the co-M1 (cold color), that with the co-VSt (hot color) and the overlapped correlation which means brain regions showed significant correlation with the both co-M1 and co-VSt (black line). During the precision grip task in the intact stage, such overlapped correlations were found only in S2/Insular (Intact in Fig.12B and Fig.13A). During the recovery stage, the number of brain regions which showed the overlapped correlations substantially increased. The sensorimotor network including the bilateral pre-SMA, co-PMv, bilateral M1v, bilateral S1, bilateral IPS, co-PG, subcortical areas such as bilateral Pu, co-Th and bilateral Cb and the limbic area such as co-OFC emerged (Recovery in Fig.12B and Fig.13B). During the whole-finger grip task in the intact stage no brain region showed the overlapped connectivity (Intact in Fig.12C and Fig.13C). On the other hand, connectivity with bilateral pre-SMA, bilateral M1d, co-S1, co-IPS and bilateral ACC emerged in the recovery stage (Recovery in Fig.12C and Fig.13D). Thus, during the whole-finger grip task brain regions which showed the overlapped connectivity with VSt and M1 did not increase as in the case of the precision grip task in the recovery stage. These results demonstrated that neuroplastic

changes in the sensorimotor-related network became tightly associated with the co-VSt during the precision grip task but less the whole-finger grip task after SCI.

VSt was essential for functional recovery of finger dexterity

In the previous study, Nishimura and colleagues have demonstrated that the reversible VSt inactivation produced deficits in finger movement during the early stage after SCI. This suggests that the VSt makes a direct contribution to the control of finger movements during the early stage after SCI (Sawada *et al.*, 2015). The current results of brain imaging study showed that the activity of VSt and the networks including the VSt and motor-related areas were both associated with functional recovery of precision grip, which suggested that the VSt was a key node of functional recovery. Despite the results of these brain imaging study and previous reversible inactivation study, whether the VSt is causally involved in the functional recovery of finger dexterity still remains elusive. I therefore made a permanent lesion of bilateral VSt before SCI in three monkeys and compared with the cases of sham lesions of VSt in other three monkeys. I first tested the effects of the permanent lesion of VSt on finger dexterity. The lesion areas completely

covered the VSt in both hemispheres. The lesion extended to the neighboring basal ganglia, such as the ventral pallidum (VP) and the rostromedial part of external and internal segments the globus pallidus (GPe and GPi, respectively) (Fig.15A). After sufficient recovery from the surgery of the injections into the VSt, none of monkeys of both the lesion and sham groups of monkeys showed impairment of the finger dexterity (VSt lesion group in Fig.15Ba, and control group in Fig.15Bb, respectively). All the six monkeys were then subjected to SCI. Lesion areas of the spinal cord were similar in both groups (Right column in Fig.16A and 16B). The monkeys started rehabilitative training of food retrieval with the affected hand from the next day of SCI. All monkeys in both groups could reach their hand to object on the first day of postoperative training, however, precision grip was impaired in two groups. The control group showed recovery of the precision grip within 60 days by daily training (Fig.16Ba), which was consistent with previous studies (Nishimur*a et al.*, 2007a, 2009, Sawada *et al.*, 2015; Tohyama *et al*. 2017).

In the VSt lesion group, recovery level of precision grip was significantly lower than that of the control group as seen in the recovery course of both groups

(Fig.16Ca). After the SCI the monkeys became unable to perform the same behavioral training as before the SCI. Therefore, I introduced an alternative training by which the monkeys were assisted to use their affected hands to hold a piece of food. Because the monkeys in the VSt lesion group couldn't retrieve a piece of food morsel through a slit for the first 2-3 weeks after SCI, the alternative training lasted 1-2 weeks longer than the control group. The precision grip in the VSt lesion group was not recovered by daily rehabilitative training for 2 months (Fig.16Aa).

On the other hand, the monkeys in the VSt lesion group gradually showed recovery of the coarse grip within approximately 2 weeks after SCI, and that grip strategy persisted throughout the entire period of observation for 2months (Fig.16Ab). The monkeys raked the food morsel out of the slit by using the index finger and then held it with the clenched hand. Similar observation was reported on the monkeys which lacked early rehabilitation for the first month after SCI (Sugiyama *et al*., 2013). Monkey Sh couldn't retrieve the food from the narrow vertical slit and showed particularly low rate of coarse grip (Fig.16Ab, red filled circles) while the coarse grip skill was gradually recovered by a different strategy which was consisted with raking and dropping the food

by his index finger, and then grasping the dropped food (Fig.16Ab, red open circles). Such behavior didn't match my criteria of the successful precision grip or coarse grip (see Methods). That was the reason why the rate of both the precision grip and the coarse grip in Monkey Sh was continuously low. However, I confirmed his skill in the coarse grip recovered because he could grasp the dropped food with a coarse grip.

In the control group, the coarse grip was observed immediately after SCI but gradually disappeared (Fig.16Bb) as seen in monkeys for PET experiment (Fig.6Bb and Fig.6Cb). The average rate of the coarse grip in the control group showed decrease, which was associated with the improvement of the rate of the precision grip (Fig.16C). However, VSt lesion group didn't show such a change in the grasping strategy (Fig.16C).

Discussion

The present study demonstrated that the VSt showed functional connectivity with motor-related networks in the performance of precision grip during the recovery process after SCI. Furthermore, the permanent lesion of the VSt did not affect the precision grip before SCI, however, impeded the recovery of precision grip, indicating the causal role of the VSt in functional recovery of finger dexterity. Together with the previous observation that reversible inactivation of the VSt impaired the high frequency component of the M1 activity (Sawada *et al.*, 2015), these results suggest that the VSt up-regulates the activity of the motor-related networks and the VSt activity is required for recovery of highly demanding dexterous finger control after SCI.

Dexterous finger movement become more demanding after SCI

The coarse grip was observed immediately after SCI but the precision grip was impaired in the pin task (Fig.6B), indicating that finger control of precision grip after SCI was more demanding than before SCI and that of coarse grip after SCI. In addition, the results in the PET imaging study showed that the VSt, which plays a critical role in

motivation-driven effort to achieve goal-oriented behaviors (Aberman and Salamone, 1999; Pessiglione *et al.*, 2007; Schmidt *et al.*, 2009, 2012), increased its activity only during the precision grip but not during the whole-finger grip in the recovery stage (Fig.7Aa and 7Ba). Furthermore, mutual functional connectivity between the co-M1 and the co-VSt emerged only during the precision grip in the recovery stage (Fig.9C, 9D, Fig.11De and 11Fe) as Mogenson *et al.* (1980) has proposed that the VSt including the NAc may be a limbic-motor interface for the translation of motivation to action initiation. A population of coritocomotoneuronal (CM) cells in the M1, which have monosynaptic connections with spinal motoneurons were reported to be selectively recruited in the execution of a precision grip, while not than that of a whole-finger grip (Muir and Lemon, 1983). The SCI model used in this study lost the direct CM connections by the CST lesion, which made precision grip highly demanding as evidenced by slower recovery of precision grip compared with coarse grip (Fig. 6Ba and 6Bd). Although the M1 activity during the precision grip was identical with that during the whole-finger grip during recovery after SCI (Fig.7Ab and 7Bb), the functional connectivity between the co-M1 and other areas including higher motor-related, subcortical motor-related areas and limbic

areas emerged particularly in the precision grip task after SCI, while those change were less in the whole-finger grip task (Fig.10). These results suggested that the co-M1 activity for the control of dexterous finger movements was supported not only by the cortical and subcortical motor network but also by the VSt and limbic cortical areas. Thus, not only behavioral results but also the imaging results showing recruitments of motor-related network and the VSt indicated that the precision grip was more demanding than whole-finger grip after SCI. These results suggested that the VSt-driven reorganization of the motor-related networks might be required for recovery of demanding finger movements after SCI. As Brodal (1973) described that the expenditure of "mental energy" depended on the severity of the paralysis, I propose that the VSt-motor related network might be underlying the neural mechanism of "mental energy".

VSt is essential for functional recovery of precision grip

A recent study has demonstrated that during the early recovery stage reversible inactivation of the VSt caused a transient deficit of amelioration in finger dexterity obtained by rehabilitation. The same manipulation caused no remarkable deficit

during the pre-SCI period and the late recovery stage (Sawada *et al.*, 2015). This previous study demonstrated the involvement of the VSt in dexterous finger control during early recovery stage, but the causal role of the VSt in recovery remains elusive. My result in the VSt-lesioned monkeys showed impairment of precision grip during early recovery stage (about 1 month after SCI) which was resembled with the previous study (Sawada *et al.*, 2015). However, its impairment maintained throughout observation period for 2 months when control monkeys showed recovery of precision grip (Fig. 16Aa and 16Ba). This result demonstrated that the VSt was essential for not only controlling of precision grip per se but also for recovery of precision grip.

It has been demonstrated that early rehabilitative training after SCI (Sugiyama *et al*., 2013) or brain injury (Biernaskie *et al*., 2004) positively influences subsequent functional recovery of finger dexterity. A case report of four SCI individuals also suggested that rehabilitative training is more effective in recovering motor performance when applied within a few days after the lesion (Winchester *et al*., 2005). Repetitive rehabilitative training on digit-use manual dexterity induces the M1 neuronal plasticity, expansion of the digit representation, with early but not delayed rehabilitative training

after brain injury (Nudo *et al*., 1996). Transient increases in the expression of plasticity-related molecules have been reported in sensorimotor cortices (SMC) including the M1, PMv, S1 during early recovery period after SCI (Higo *et al.*, 2009). Furthermore, during early recovery stage after SCI, the VSt up-regulates activity of the SMC and is directly involved in the control of finger movements (Sawada *et al.*, 2015). Thus, starting rehabilitative training early is very important for inducing plastic change in motor-related areas and functional recovery. From these evidences, during early recovery stage the lack of facilitation of the motor-related areas by the VSt due to its lesion might prevent the reorganization in the motor-related network required for functional recovery of precision grip. In contrast, the coarse grip, immature dexterous finger movement, recovered even in the VSt lesioned monkeys. This would be related to the less effect of the VSt on the reorganization of the motor-related network required for a whole-finger grip throughout recovery stage (Fig.12C). Furthermore, my results indicate that the VSt activity affect not only M1 but also other motor-related regions, and might be critical to strengthen the motor-related networks required for the recovery of precision grip after SCI (Fig.11-13, and Table.5).

Possible mechanism of functional connectivity in the VSt-motor network

It is important to consider how the M1 and the VSt concurrently increased functional connectivity with the same brain areas in the motor-related network. Anatomical evidence that supports the above question remains unclear. The M1 directly and/or multisynaptically receives abundant projections from extensive cortical areas (e.g. frontal cortical area) and subcortical areas (e.g. basal ganglia) (Miyachi *et al.*, 2005). Therefore, it is reasonable that the M1 increased functional connectivity with other cortical and subcortical areas (e.g. OFC, pre-SMA, PMv, SMA, IPS, Pu, Th). Mogenson *et al.* (1980) has proposed that the VSt may be a limbic-motor interface, involved in translation from motivation to action. The VSt receives inputs from the limbic system (e.g. OFC) involved in the processing motivation (Haber *et al.*, 1995), then directly projects to the VP and/or mono- or multi-synaptically projects to cortical- and subcortical-motor related networks (Alexander *et al.*, 1986; Haber *et al.*, 1990; Haber, 2003; Kelly and Strick, 2004; Miyachi *et al.*, 2005; Haber and Knutson, 2010). Therefore, it would be possible for the VSt to affect activity of the motor-related areas concurrently with M1

recruited in the execution of the demanding dexterous finger control after SCI.

Methodological limitation

As a methodological limitation of this study, I couldn't make the lesion confined to the VSt (Fig.15A). I observed that lesion area extended to the VP and a rostromedial part of the GPe-GPi in all the three monkeys belonging to the VSt lesion group. The VP and a rostomedial part of the GPe-GPi receives direct projections from the VSt (Haber *et al*., 1990, Haber and Knutson, 2010). Furthermore, a growing body of work has revealed that the VP and a rostral part of GPe-GPi have a similar function to the VSt (Pessiglione *et al.*, 2007; Schmidt *et al.*, 2009, 2012; Smith *et al.*, 2009; Tachibana and Hikosaka, 2012; Richard *et al.*, 2016). Not only the VSt but also these areas might be involved in the present results. More precise lesion study will be needed to confirm the responsibility of the VSt in functional recovery.

Clinical implication

Clinical studies have showed that depression is the most frequently occurs after

SCI or stroke (Elliot *et al.*, 1966; Morris *et al.*, 1990). Several studies have revealed that depressive states were associated with severity of residual motor function, functional recovery and activities daily life (Saxena *et al*., 2007; Chemerinski *et al*., 2012; Shin *et al*., 2012). These clinical reports suggest that improving depressive mental status after neuronal damage may facilitate functional recovery. In addition, it has noted that patients with depression (Cléry-Melin *et al.*, 2011) or Parkinson's disease (Chong *et al*., 2015) show reduced high-effort motor exertion (e.g. lower force output involving hand grip). Therefore, up-regulation of the VSt, which would drive motor-related network, might improve not only psychological problems but also motor function, then, might facilitate functional recovery. Future studies investigating what kind of psychological approaches (e.g. encouragement, praise) can activate the VSt are required to promote the development of effective rehabilitation.

Tables and legends

Table 3: Statistical analysis of the rCBF increase related to functional recovery during the precision grip task and the whole-finger grip task in the recovery stage compared with that in the intact stage.

Precision grip (cluster size > 250, $P < 0.01$, t-value > 2.33)

Brain region	Laterality	t-value	x	y	z	Remarks
Recovery > Pre-SCI						
VSt	Contra	2.894	86	72	44	
M1 (ventral)	Contra	3.984	61	91	83	Extend to S1
S2	Contra	2.815	49	99	70	
V2	Contra	2.764	53	135	68	
V2/V3v	Contra	3.136	47	141	48	
V2	Contra	3.209	75	149	87	
V1	Ipsi	3.014	128	148	66	
Cb vermis	Mid	3.501	92	153	32	

Whole-finger grip (cluster size > 250, $P < 0.01$, t-value > 2.33)

Brain region	Laterality	t-value	x	y	z	Remarks
Recovery > Pre-SCI						
TPPro	Contra	2.76	63	76	30	
Amygdala	Contra	3.843	84	83	27	
TE1/TE2	Ipsi	3.895	128	81	23	
VP/Amygdala	Ipsi	3.684	111	80	42	
Insular/S2	Contra	3.064	56	80	54	
M1 (ventral)	Contra	4.42	60	90	87	Extend to PMv, S1
S1	Ipsi	2.705	135	95	91	
S1	Contra	3.58	51	97	79	
S2	Contra	3.277	42	102	65	

TEa/TPO	Contra	2.918	46	107	41	
PFG	Ipsi	3.047	138	110	91	
PG (rostral)	Ipsi	2.944	137	118	92	
PG (caudal)	Ipsi	2.727	133	131	95	
TEOM	Contra	2.828	43	123	70	
TEO	Contra	3.344	40	128	43	
V2/V3v	Contra	2.781	49	141	59	Extend to V1
V1	Ipsi	3.715	119	151	96	

The level of the coefficients was set at $P < 0.01$ ($t > 2.33$). t-values at the center of individual masses of activation (the locations are indicated with the positions along the x-, y- and z-axis) are indicated.

Table 4: Statistical analysis of correlation of the rCBF in the co-M1 with that in other brain regions during the intact and the recovery stages.

Precision grip (cluster size > 250, $P < 0.01$)

Brain region	Laterality	t-value	x	y	z	Remarks
Pre (t > 2.38)						
Area 14m	Ipsi	3.427	97	44	45	
OFC	Contra	4.017	74	42	57	
rACC	Contra	3.243	89	47	57	
Area 46	Contra	3.217	69	52	72	
cACC	Ipsi	2.981	104	62	73	
PMd	Contra	2.981	74	70	90	
SMA	Contra	3.401	89	72	90	
Amygdala	Contra	3.112	88	90	31	
Globus pallidus	Ipsi	3.374	113	87	47	
M1 (ventral)	Contra	37.59	60	92	84	Extend to S1, S2. Insular
S2	Ipsi	3.073	138	98	68	
Putamen	Contra	3.578	63	99	59	
PCC	Contra	3.468	80	104	82	
V1	Ipsi	2.945	128	135	61	
Cb	Ipsi	3.615	125	130	34	
Cb	Ipsi	3.991	100	141	21	
Cb	Ipsi	2.615	110	147	26	
Cb	Mid	2.798	95	149	45	
Cb	Ipsi	3.318	110	154	37	
Cb vermis	Mid	2.78	92	155	30	
Recovery (t > 2.35)						
OFC	Contra	3.972	74	36	62	
Pre-SMA	Mid	3.549	95	64	91	
SMA	Mid	3.145	97	77	98	

SMA/M1 (medial)	Mid	3.113	96	90	95	
VSt	Mid	4.54	95	74	42	
PMv	Contra	2.594	64	75	68	
TE1	Contra	3.291	63	75	15	
Putamen	Ipsi	3.619	126	91	60	
Putamen	Contra	4.224	70	95	63	
Insular	Ipsi	2.515	134	97	58	
M1 (dorsal)	Ipsi	3.488	123	89	93	
M1 (ventral)	Ipsi	3.362	129	91	83	
S1	Ipsi	3.396	129	105	80	
M1 (dorsal)	Ipsi	3.016	102	107	103	
M1 (ventral)	Contra	58.72	60	91	83	Extend to S1, posterior parietal area, S2, Insular
Thalamus	Contra	4.5	79	106	61	
MIP	Ipsi	3.632	103	130	95	
LIP/MIP	Contra	3.041	71	129	92	
V4v/V3v	Contra	4.277	57	131	47	
Cb	Contra	3.199	79	122	43	
Cb	Ipsi	4.737	107	153	40	
Cb	Contra	4.25	82	147	32	
Cb vermis	Contra	3.724	87	152	61	
Cb	Ipsi	2.954	123	156	32	

Whole-finger grip (cluster size > 250, $P < 0.01$)

Brain region	Laterality	t-value	x	y	z	Remarks
Pre (t > 2.38)						
OFC	Ipsi	4.187	111	39	58	
PMv	Contra	3.112	67	72	72	
Putamen	Ipsi	3.099	111	81	60	
S2/Insular	Ipsi	3.571	126	97	73	Extend to S1
SMA	Ipsi	3.037	103	85	91	
cACC/SMA	Contra	4.554	79	88	84	

M1 (ventral)	Contra	36.3	60	92	84	Extend to S1, S2, Insular
S1	Contra	3.761	74	104	85	Extend to VIP, MIP, LIP. AIP
S2/Insular	Contra	3.495	56	101	74	
M1 (dorsal)	Ipsi	3.5	107	103	94	
Thalamus	Ipsi	3.771	110	104	54	
Thalamus	Contra	2.737	83	94	62	
PCC	Contra	3.972	85	115	79	
PE/MIP	Ipsi	3.716	113	117	96	
DpMe	Contra	3.881	82	117	48	
PaAC	Contra	2.863	59	119	72	
TPO	Contra	2.734	60	128	73	
PGM	Ipsi	3.068	99	128	89	
V2	Contra	3.378	79	147	68	
Cb	Ipsi	2.963	97	125	50	
Cb	Ipsi	4.213	124	136	35	
Cb	Ipsi	4.187	104	148	25	
Cb	Contra	3.835	84	150	25	
Cb	Mid	3.236	97	155	56	
Cb vermis	Mid	4.436	97	168	49	
Recovery (t > 2.35)						
OFC	Contra	3.79	70	57	49	
cACC	Ipsi	2.95	99	66	71	
Pre-SMA	Mid	4.09	96	69	91	
Caudate	Ipsi	2.84	104	92	68	
Thalamus	Mid	3.3	93	92	57	
M1 (dorsal)	Ipsi	5.436	114	89	98	
M1 (ventral)	Contra	53.86	60	91	84	Extend to PM, S1, posterior parietal area, S2, Insular
M1 (medial)	Mid	3.368	94	89	94	
PG/PE/LIP/MIP	Contra	2.701	47	119	86	
MT	Contra	3.051	50	119	60	

PGOp/PaAC	Ipsi	3.134	136	118	77
PE/MIP	Ipsi	2.867	115	116	94
Cb	Contra	3.074	87	137	55
Cb	Contra	4.513	69	145	27
Cb vermis	Contra	2.951	89	156	44

The level of the coefficients was set at $P < 0.01$ ($t > 2.38$ for the intact stage, $t > 2.35$ for the recovery stage). *t*-values at the center of individual masses of correlation (the locations are indicated with the positions along the x-, y- and z-axis) are indicated.

Table 5: Statistical analysis of correlation of the rCBF in the co-VSt with that in other brain regions during the intact and the recovery stages.

Precision grip (cluster size > 250, $P < 0.01$)

Brain region	Laterality	t-value	x	y	z	Remarks
Pre (t > 2.38)						
OFC	Ipsi	3.688	122	52	59	
OFC	Contra	4.751	56	54	49	
rACC	Contra	3.309	88	55	64	
Area 45B	Contra	2.902	69	64	65	
Putamen/VSt	Ipsi	4.109	115	73	45	
VSt	Contra	32.35	85	72	43	Extend to Putamen
S2/insular	Contra	3.083	63	91	70	
TPO	Ipsi	3.239	148	110	61	
Pontine nuclei	Ipsi	2.872	102	119	26	
TEO	Ipsi	2.908	147	120	51	
V4d	Contra	3.184	49	130	67	
V2/V3d	Ipsi	2.954	143	135	65	
V1/V2	Ipsi	2.936	143	142	73	
V3d/V4d	Ipsi	2.624	132	144	75	
V1	Contra	3.037	48	148	51	
V1	Ipsi	2.587	119	162	67	
V1/Cb vermis	Mid	3.376	96	164	61	
V2	Ipsi	2.927	129	161	60	
V1	Ipsi	2.642	114	167	69	
V1	Contra	3.44	87	172	62	
Recovery (t > 2.35)						
Area 46	Contra	3.214	82	34	59	
OFC	Contra	3.471	75	44	62	
OFC	Ipsi	3.123	105	42	55	

Area 46v	Ipsi	2.739	120	44	66	
Area 46v	Ipsi	2.812	121	53	70	
rACC	Ipsi	3.018	97	47	69	
pre-SMA	Mid	4.632	91	63	88	
Putamen	Contra	3.422	71	74	46	
PMv	Contra	4.158	63	75	71	
VSt	Contra	40.86	85	72	44	Extend to Putamen
SMA	Ipsi	2.765	100	72	95	
Caudate	Contra	2.61	84	81	63	
Caudate	Ipsi	4.31	102	84	70	
Putamen	Ipsi	3.152	129	83	54	
Putamen	Contra	3.158	66	84	61	
Insula/S2	Ipsi	3.226	132	86	58	
M1 (ventral)	Ipsi	3.387	131	90	82	
S1	Ipsi	3.684	132	101	82	
S1	Contra	4.796	67	102	83	
M1 (ventral)	Contra	2.608	61	91	83	Extend to S2/Insular
RN/Reticular formation	Contra	3.647	82	103	47	
Thalamus	Contra	3.807	79	106	60	
TPO	Contra	3.982	56	105	53	
PG/PGOp	Contra	2.566	55	118	87	
TPO	Contra	2.681	64	123	72	
MIP/LIP	Ipsi	3.036	110	129	95	
MIP/LIP	Ipsi	2.819	110	139	91	
MIP/LIP	Contra	3.464	83	143	97	
V4v	Ipsi	2.899	134	135	44	
V1	Contra	3.79	83	161	62	
V1	Ipsi	2.805	121	157	69	
V1	Contra	2.393	84	156	90	
Cb	Contra	2.935	72	154	30	
Cb	Ipsi	3.478	119	155	35	
Cb	Contra	4.109	81	158	48	

Whole-finger grip

Brain region	Laterality	t-value	x	y	z	Remarks
Pre (t > 2.38)						
Area 14m/14o	Ipsi	2.881	100	37	53	
Area 9m	Mid	2.541	94	41	76	
rACC	Mid	2.872	97	45	63	
Clustrum	Contra	2.734	63	72	49	
VSt	Contra	28.98	85	72	43	Extend to Putamen, Caudate
Caudate	Ipsi	3.147	110	83	73	
TLR	Contra	3.009	70	102	18	
PPTg	Ipsi	2.853	105	114	39	
V2	Ipsi	2.623	98	159	74	
V2	Contra	3.147	87	163	67	
Recovery (t > 2.35)						
OFC	Contra	2.879	69	43	61	
cACC	Mid	4.276	94	62	76	Extend to pre-SMA
Area 9/46	Contra	3.259	70	62	74	
VSt	Contra	39.91	85	72	44	Extend to Caudate, Putamen
VSt	Ipsi	3.18	106	72	43	
ST1/TPPro	Contra	3.005	55	73	24	
Putamen	Contra	3.834	67	78	52	
Caudate	Contra	3.337	73	95	73	
M1 (ventral)	Ipsi	3.512	125	91	86	Extend to S1
M1 (dorsal)	Ipsi	3.102	101	91	97	
M1 (dorsal)	Contra	3.76	80	94	92	
PCC	Mid	3.862	98	95	80	
S1	Ipsi	3.572	118	107	103	
VIP/LIP/MIP	Contra	4.086	69	111	83	
PECg	Contra	2.866	79	113	80	
V4v	Ipsi	3.196	134	133	42	

V6	Contra	3.203	92	148	88
V2/V1	Contra	3.79	74	147	58
V2/V3d	Ipsi	4.15	126	155	58
Cb	Ipsi	2.5	107	143	51
Cb	Ipsi	3.313	108	148	24
Cb/V2	Contra	3.52	89	165	57

The same arrangement as Table 4.

Abbreviations for Table 3-5: Area 14m, medial part of area 14; Area 14o, orbital part of area 14; Area 9m, medial part of area 9; Area 46v, ventral part of area 46; OFC, orbitofrontal cortex; rACC, rostral part of anterior cingulate cortex; cACC, caudal part of anterior cingulate cortex; PCC, posterior cingulate cortex; VSt, ventral striatum; VP, Ventral pallidum, PMd, dorsal premotor area; PMv, ventral premotor area, pre-SMA, pre-supplementary motor area; SMA, supplementary motor area; M1, primary motor cortex; S1, primary somatosensory cortex; S2, secondary somatosensory cortex; MIP, medial intraparietal area; LIP, lateral intraparietal area; VIP, ventral intraparietal area; PaAC, caudal part of paraauditory area, PE, parietal area PE; PECg, cingulate part of parietal area PE; PFG, parietal area PFG; PG, parietal area PG; PGM, medial part of parietal area

PF; PGOp, opercular part of parietal area PF; ST1, superior temporal sulcus area 1; TPPro, temporopolar proisocortex; TE1, temporal area TE1; TE2, temporal area TE2; TEa, temporal area TEa; TEO, occipital part of temporal area TE; TEOM, occipitomedial part of temporal area TE; TLR, rostral part of temporal area TL; TPO, temporal parieto-occipital associated area; V1, primary visual cortex; V2, visual area 2; V3d, dorsal part of visual area 3; V3v, ventral part of visual are 3, V4d, dorsal part of visual area 4; V4v, ventral part of visual area 4, V6, visual area 6; MT, meddle temporal visual area; DpMe, deep mesencephalic nucleus; RN, red nucleus; PPTg, pedunculopontine tegmental nucleus; Cb, cerebellum

Figures and legends

Figure 6

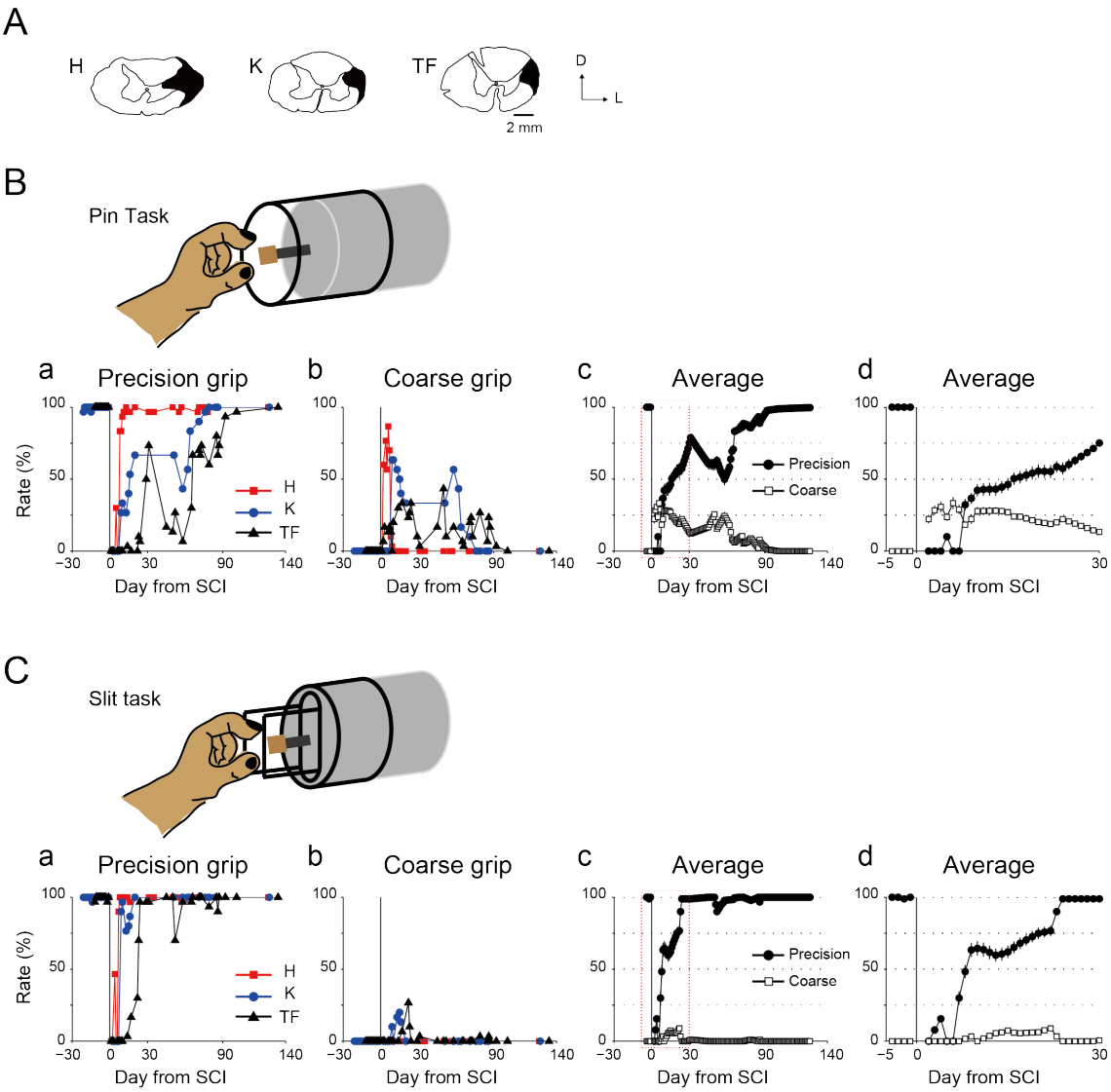

Figure 6: Recovery time course after SCI in the monkeys used for the PET experiments. (**A**): Illustrations of coronal spinal cord sections indicate lesion extent (black hatch) of the l-CST at the C4/C5 segment in individual monkeys. Illustrations of Monkey H was flipped because of opposite lesion side compared with other monkeys.

Illustrations were modified from the previous study (Nishimura *et al*., 2007a). D, dorsal; L, lateral. (**B**): Performance of the pin task, (a) the precision grip, (b) the coarse grip in individual monkeys. (c) Average rate in the precision and coarse grip, (d) Expansion of red square range showing in (c). (**C**): Performance of the slit task, (a) the precision grip, (b) the coarse grip in individual monkeys. (c) Average rate in the precision and coarse grip, (d) Expansion of red square range in (c). Error bars in (Bc), (Bd), (Cc) and (Cd) indicate SEM (standard error of the mean).

Figure 7

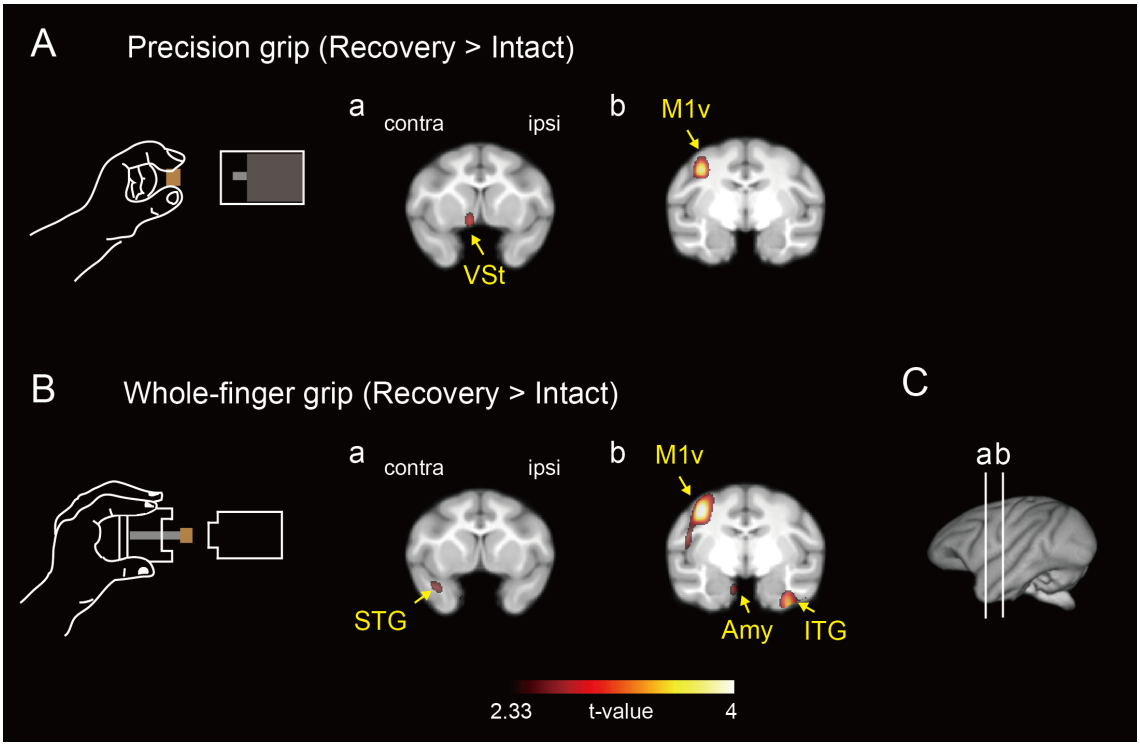

Figure 7: Increased brain activation related to functional recovery during the precision grip task and the whole-finger grip task. (**A**): The precision grip task. (**B**): The whole-finger grip task. Results were obtained from averaged data from the three monkeys. Brain areas with significantly increased rCBF ($P < 0.01$, uncorrected for multiple comparison) were superimposed on a template brain MRI of macaque monkeys (see also Fig.8). The significant level was given in terms of t-values represented on a color scale. (**C**): Lines (a) and (b) indicate the levels of coronal sections of (a) and (b) in (**A**) and (**B**). Abbreviations: contra, contralesional; ipsi, ipsilesional; VSt, ventral

striatum; M1v, ventral aspect of the primary motor cortex; Amy, amygdala; STG, superior temporal gyrus; ITG, inferior temporal gyrus.

Figure 8

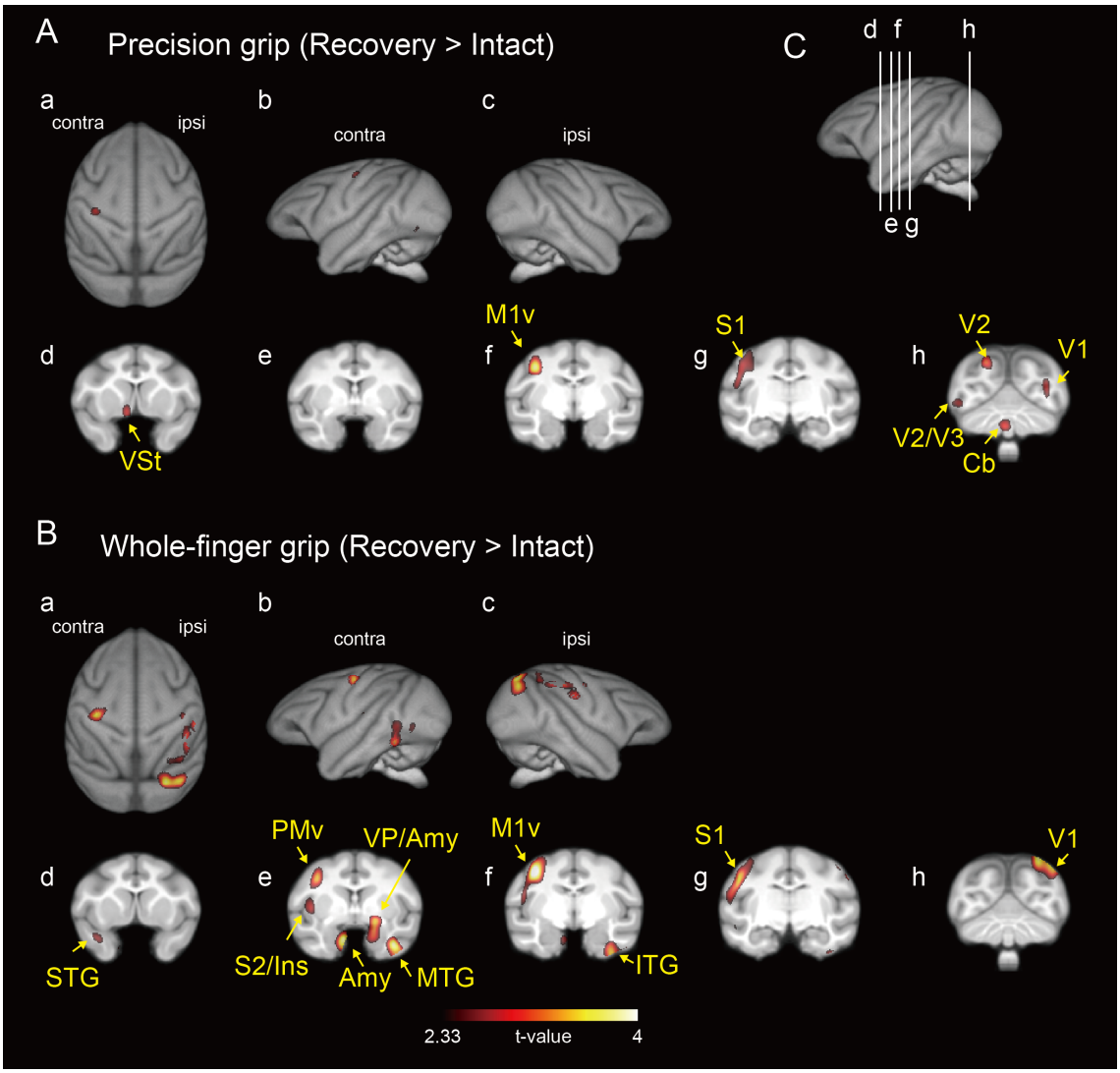

Figure 8: Increased brain activation related to functional recovery. (**A**): Precision grip task. (**B**): Whole-finger grip task. Results were obtained from the three monkeys and averaged. Brain areas with significantly increased rCBF ($P < 0.01$, uncorrected for multiple comparison) were superimposed on a template brain MRI of macaque monkeys. The significant level was given in terms of t-values represented on a color scale. (**C**):

Lines (d) - (h) indicate the levels of coronal sections of (d) - (h) in (**A**) and (**B**). Abbreviations: contra, contralesional; ipsi, ipsilesional; VSt, ventral striatum; PMv, ventral pre-motor area; M1v, ventral aspect of the primary motor cortex; S1, primary somatosensory cortex; S2, secondary somatosensory cortex; Ins, Insular cortex; Amy, amygdala; STG, superior temporal gyrus; MTG, middle temporal gyrus; ITG, inferior temporal gyrus, V1, primary visual cortex; V2 and V3, visual area 2 and 3; Cb, cerebellum.

Figure 9

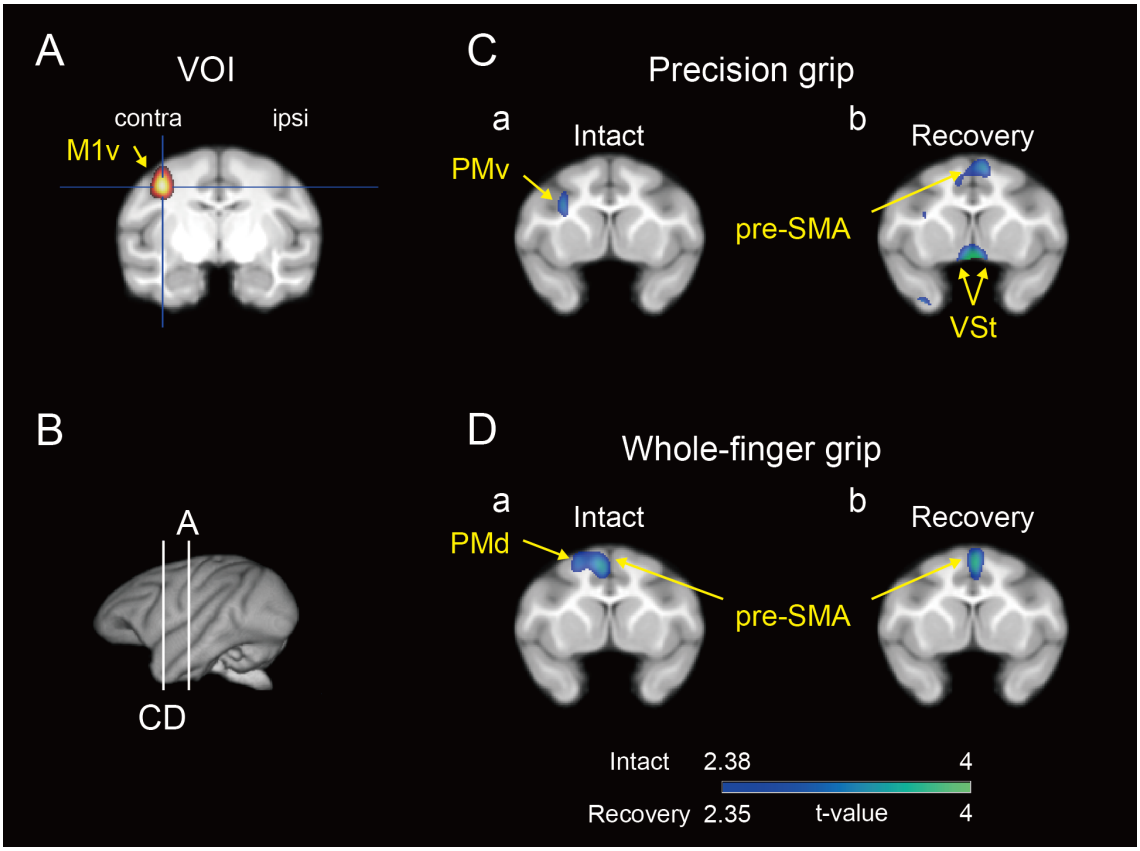

Figure 9: Functional connectivity between M1 and VSt during recovery. (**A**): Voxels of interests (VOI) for the ventral aspect of contralesional M1 (co-M1v) were determined by the results of the main effect of the functional recovery showing in Fig. 7A. (**B**): Vertical lines indicate the levels of coronal sections in (**A**), (**C**) and (**D**). (**C, D**): Brain areas having a significant positive correlation with the co-M1 during (**C**) the precision grip task and during (**D**) the whole-finger grip task were indicated by cold colors ($P <$ 0.01, uncorrected for multiple comparison) in (a) the intact stage and (b) the recovery

stage. Average data obtained from the three monkeys. Brain area which showed positive correlation with the co-M1v were superimposed on a template brain MRI (see also Fig.10).

Figure 10

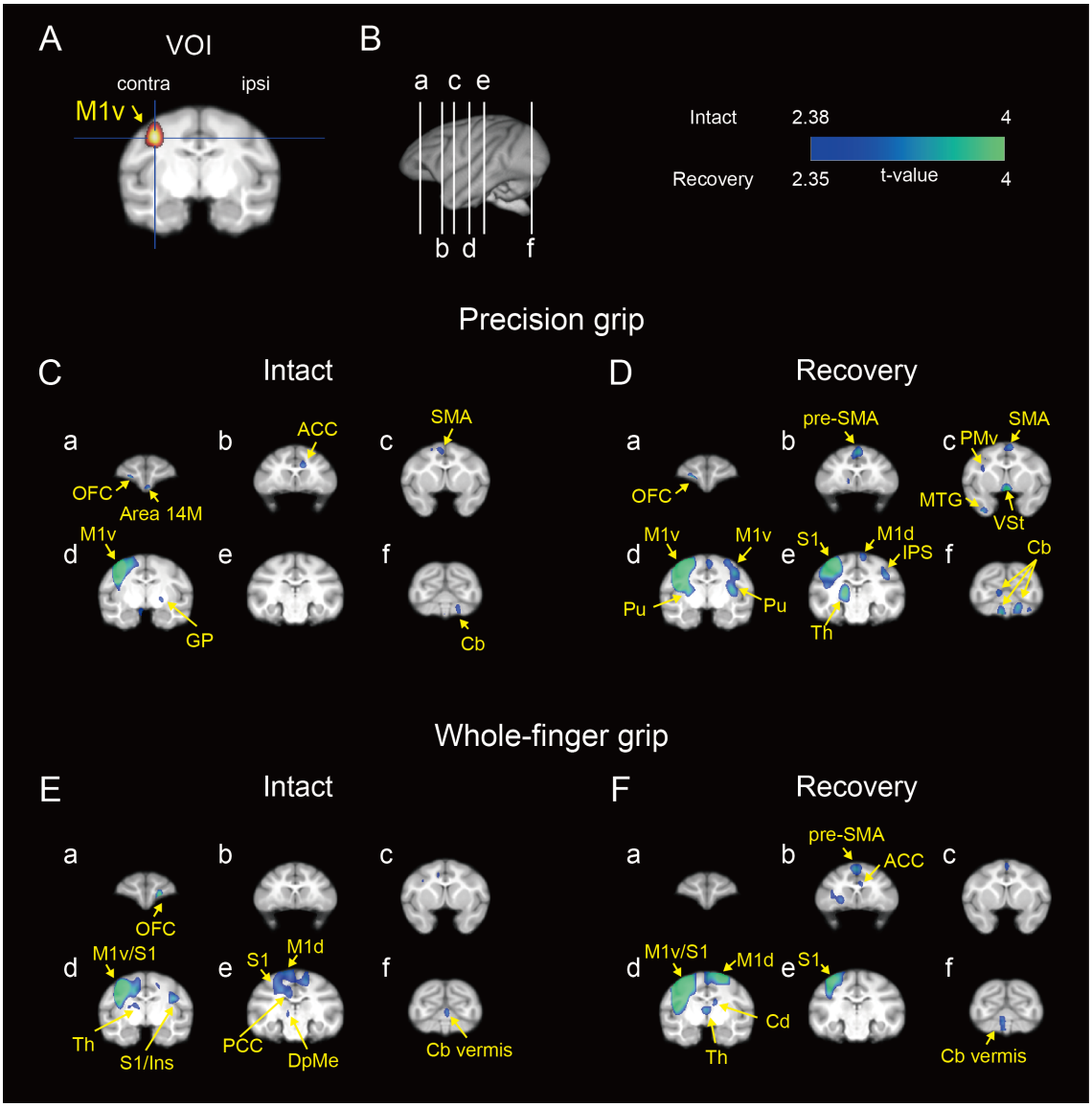

Figure 10: Functional connectivity of with the contralesional M1 before and after SCI. (**A**): VOI of in the ventral aspect of contralesional M1 (co-M1v). The correlations were calculated between the rCBF value of the VOI in the co-M1v and that in other regions during the behavioral task. Brain areas that have significant positive correlation

($P < 0.01$, uncorrected for multiple comparisons) were shown on a template brain MRI. (**B**): Lines (a) - (f) indicate the levels of coronal sections of (a) - (f) in (**C**) - (**F**). (**C**, **D**): The precision grip task (**C**) before and (**D**) after SCI. (**E**, **F**): The whole-finger grip task (**E**) before and (**F**) after SCI. The significance level was given in terms of t-values represented in a colored scale. Abbreviations: contra, contralesional; ipsi, ipsilesional; OFC, orbitofrontal cortex, ACC, anterior cingulate cortex; VSt, ventral striatum; Pu, putamen; Cd, caudate nucleus; GP, globus pallidus; pre-SMA, pre-supplementary motor area; SMA, supplementary motor area; PMv, ventral premotor area; M1v, ventral aspect of the primary motor cortex; M1d, dorsal aspect of the primary motor cortex; S1, somatosensory motor cortex; Ins, Insular cortex; PPC, posterior cingulate cortex; Th, thalamus; DpMe, deep mesencephalic nucleus; IPS, intraparietal sulcus, Area 14M, Brodmann area 14 medial part; MTG, middle temporal gyrus; V2, V3, visual area 2 and 3; Cb, cerebellum.

Figure 11

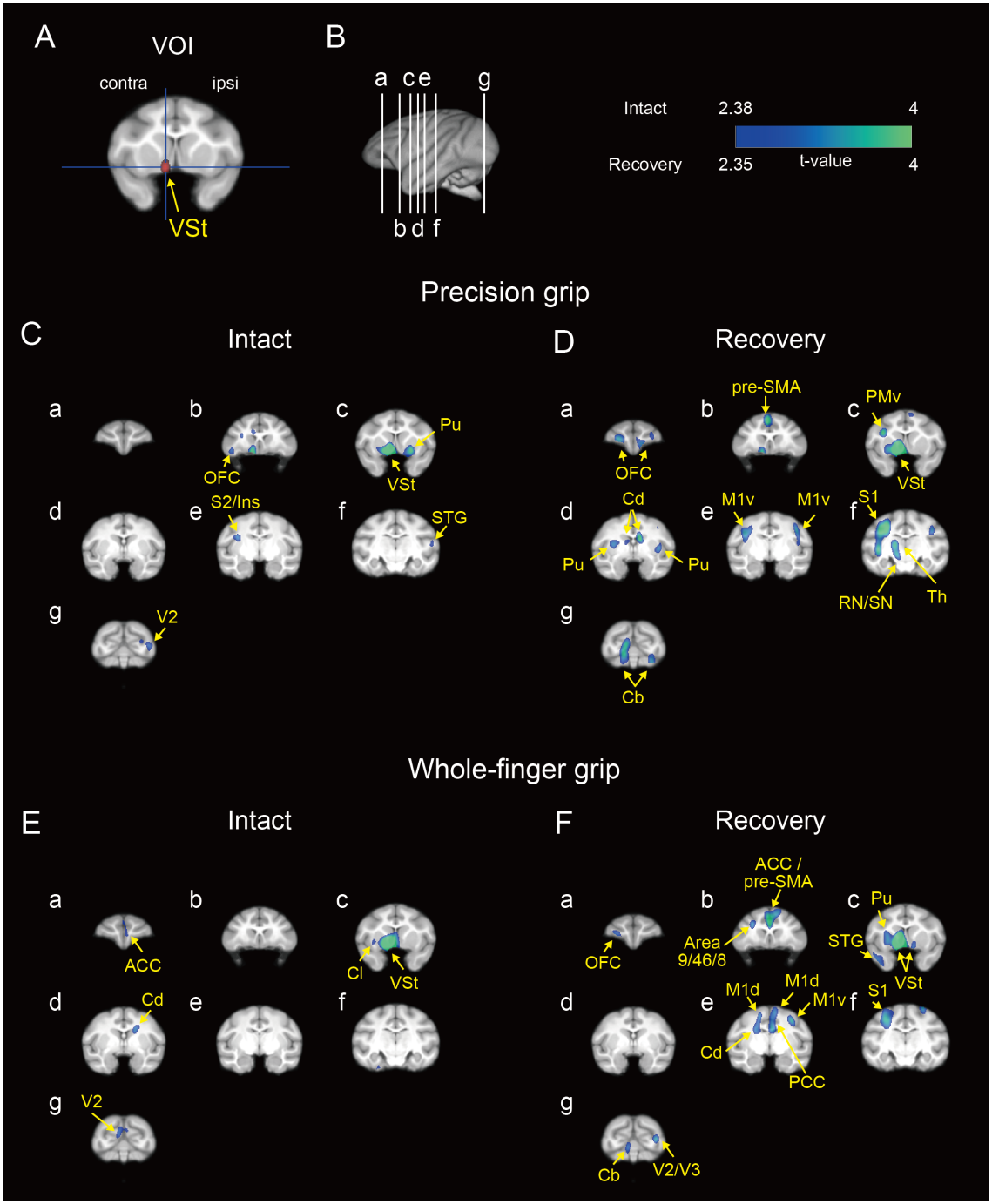

Figure 11: Functional connectivity with the contralesional VSt before and after SCI.

(**A**): VOI of contralesional VSt (co-VSt). The correlations were calculated between the

rCBF value of the VOI in co-VSt and that in other regions during the behavioral task. Brain areas that have significant positive correlation ($P < 0.01$, uncorrected for multiple comparisons) were indicated on a template brain MRI. (**B**): Lines (a) - (g) indicate the levels of coronal sections of (a) - (g) in (**C**) - (**F**). (**C, D**): The precision grip task (**C**) before and (**D**) after SCI. (**E, F**): The whole-finger grip task (**E**) before and (**F**) after SCI. The significance level was given in terms of t-values represented a colored scale. Abbreviations: contra, contralesional; ipsi, ipsilesional; OFC, orbitofrontal cortex, ACC, anterior cingulate cortex; Cl, claustrum; VSt, nucleus accumbens; Pu, putamen; Cd, caudate nucleus; pre-SMA, pre-supplementary motor area; PMv, ventral premotor area; M1v, ventral aspect of the primary motor cortex; M1d, dorsal aspect of the primary motor cortex; S1, somatosensory motor cortex; S2, secondary somatosensory cortex; Ins, Insular cortex; RN, red nucleus; SN, substantia nigra; Th, thalamus; CG, cingulate gyrus; Area 8, 9, 24 and 46, Brodmann area 8, 9, 24 and 46; STG, superior temporal gyrus; V2, V3, visual area 2 and 3; Cb, cerebellum.

Figure 12

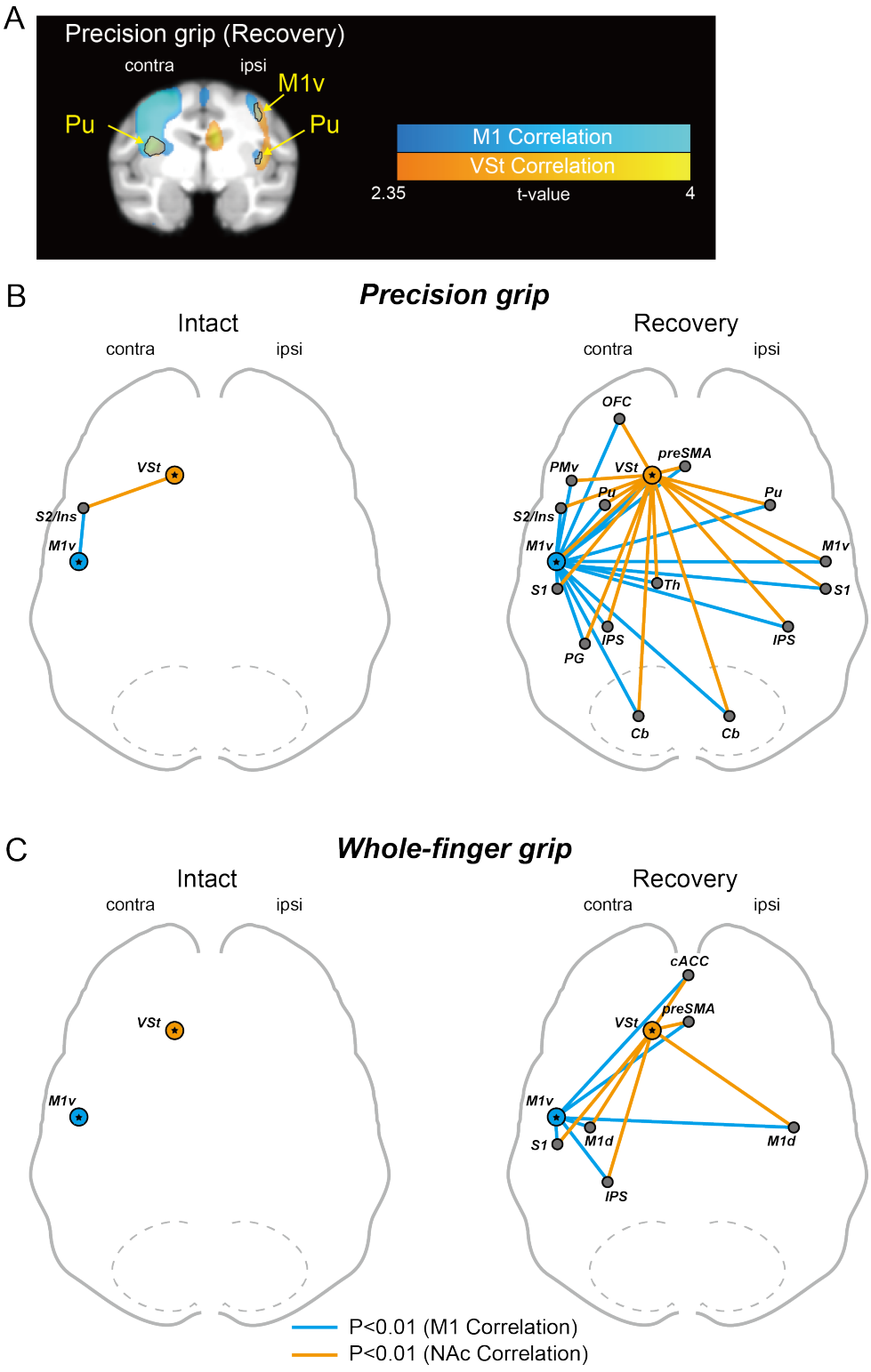

Figure 12: Overlapped functional connectivity between the M1 network and VSt

network. (**A**): Example of overlapped functional connectivity. Brain regions showed overlapped functional connectivity with the M1 and VSt shown by black outlines. Brain regions showed functional connectivity with the M1 and the co-VSt network were indicated by cold color or hot color, respectively. (**B**, **C**): The functional connectivities with both co-VSt and co-M1 during (**B**) the precision grip task and (**C**) the whole-finger grip task before and after SCI. Note that only brain areas having significant connectivities with both the co-M1 and the co-VSt were shown in these schemes (see also Fig.13). Light blue lines indicate significant functional connectivities with co-M1. Orange lines indicate significant functional conectivities with co-VSt. Abbreviations: OFC, orbitofrontal cortex; pre-SMA, pre-supplementary motor area; Pu, putamen; S2, the secondary somatosensory cortex; Ins, Insular cortex; IPS, intraparietal sulcus; PG, PG in the posterior parietal cortex; Th, thalamus; Cb, cerebellum; cACC, caudal anterior cingulate cortex; M1d, dorsal aspect of the primary motor cortex.

Figure 13

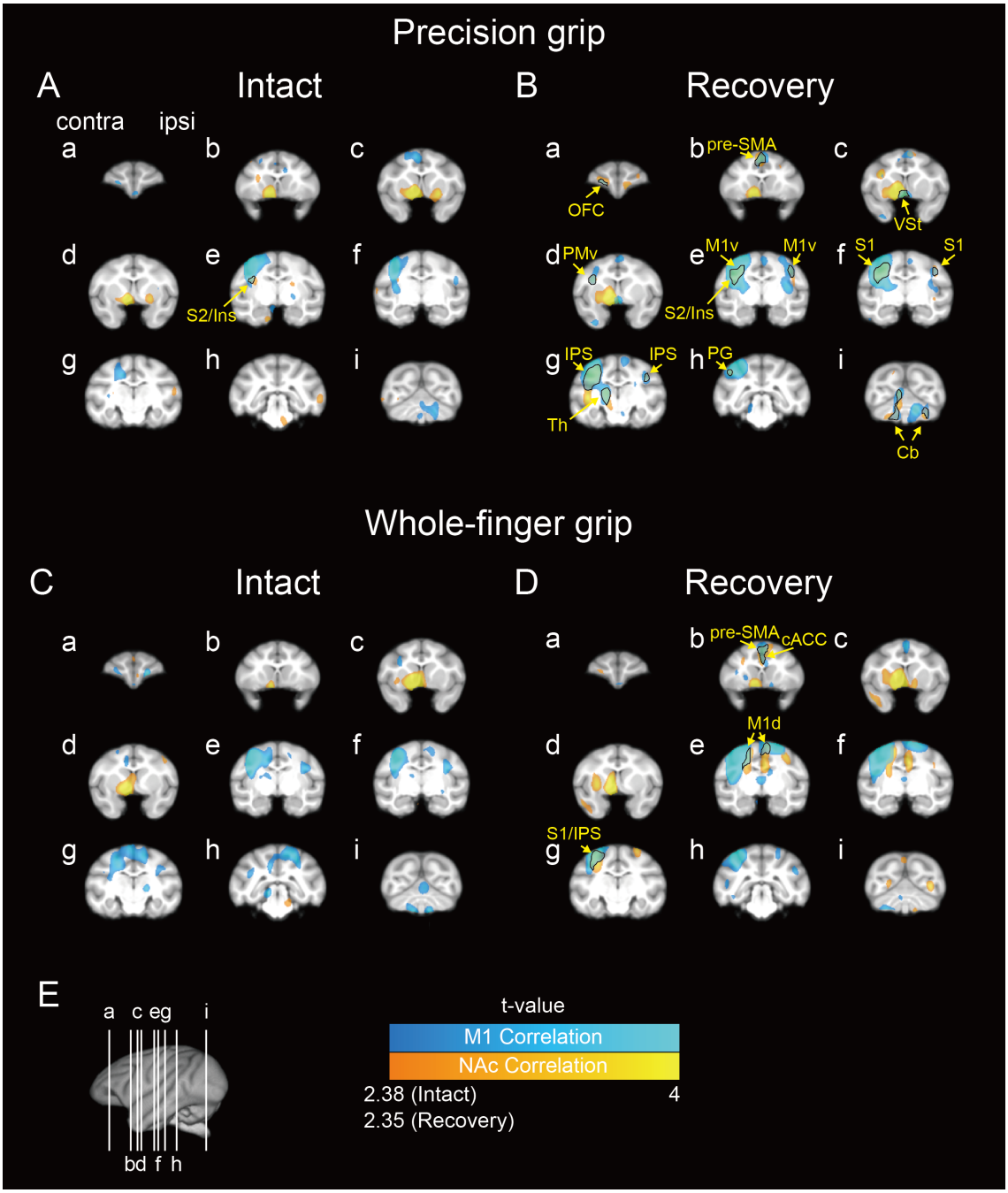

Figure 13: Overlapped functional connectivity between the M1 and VSt. Brain regions revealing overlapped functional connectivity with the M1 and VSt were shown

by black outlines. Brain regions with the M1 and the co-VSt network were indicated by cold color or hot color respectively. (**A**, **B**): The precision grip task (**A**) before and (**B**) after SCI. (**C**, **D**): The whole-finger grip task (**C**) before and (**D**) after SCI. The significance level was given in terms of t-values represented a colored scale. (**E**): Lines (a) - (i) indicate the levels of coronal sections of (a) - (i) in (**A**) - (**D**). Abbreviations: OFC, orbitofrontal cortex, cACC, caudal anterior cingulate cortex; VSt, ventral striatum; pre-SMA, pre-supplementary motor area; PMv, ventral premotor area; M1v, ventral aspect of the primary motor cortex; M1d, dorsal aspect of the primary motor cortex; S1, somatosensory motor cortex; S2, secondary somatosensory cortex; Ins, Insular cortex; IPS, intra parietal sulcus; PG, PG in the posterior parietal cortex; Th, thalamus; Cb, cerebellum.

Figure 14

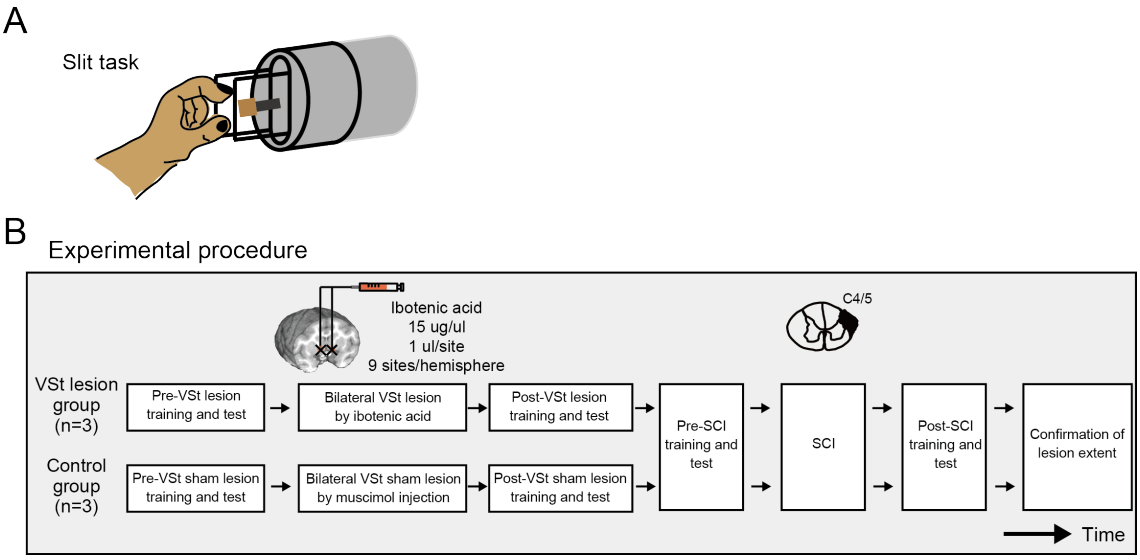

Figure 14: The experimental design of the VSt lesion study. (**A**): Illustration of behavioral task (Slit task) for assessment of the finger dexterity. (**B**): Procedure in the VSt lesion experiment. All monkeys in the VSt lesion group and the control group were trained and tested before and after the bilateral VSt lesion or sham lesion and after SCI, respectively. At the end of the experiment the extent of the VSt lesion and the spinal cord lesion was confirmed by histological analyses.

Figure 15

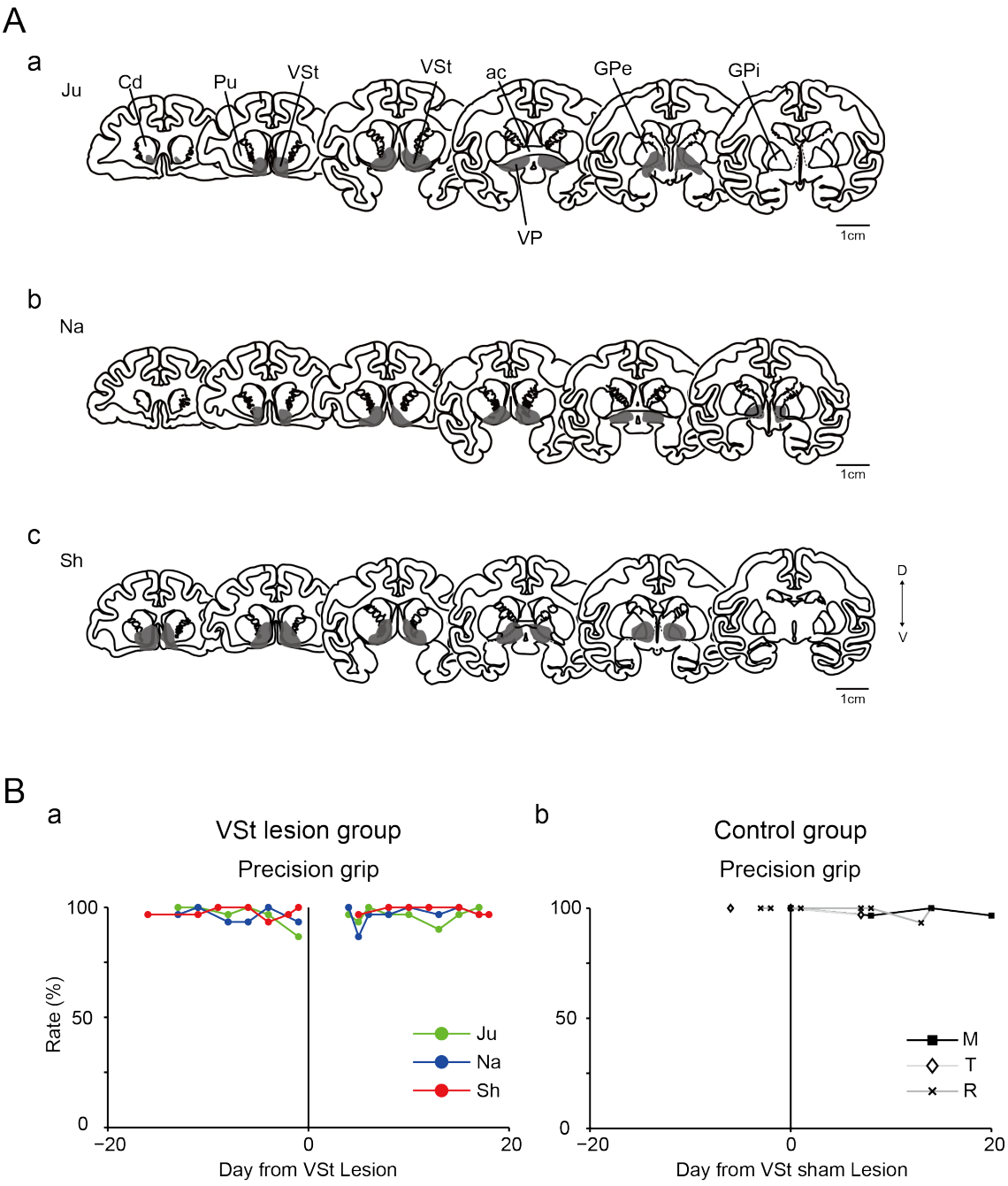

Figure 15: The lesion extent of VSt and effect of VSt lesion on the finger dexterity.

(**A**): The extent of the VSt lesion. Six representative coronal sections through the VSt are arranged rostro-caudally for each monkey [Monkey Ju (a), Na (b) and Sh (c)]. The grey

hatch indicates the lesion area. Abbreviations: Cd, caudate nucleus; Pu, putamen; VSt, ventral striatum; ac, anterior commissure; VP, ventral pallidum; GPe, external globus pallidus; GPi, internal globus pallidus; D, dorsal; V, ventral. (**B**): Rate of the precision grip before and after the VSt or sham lesion. (a) VSt lesion group, (b) Control group.

Figure 16

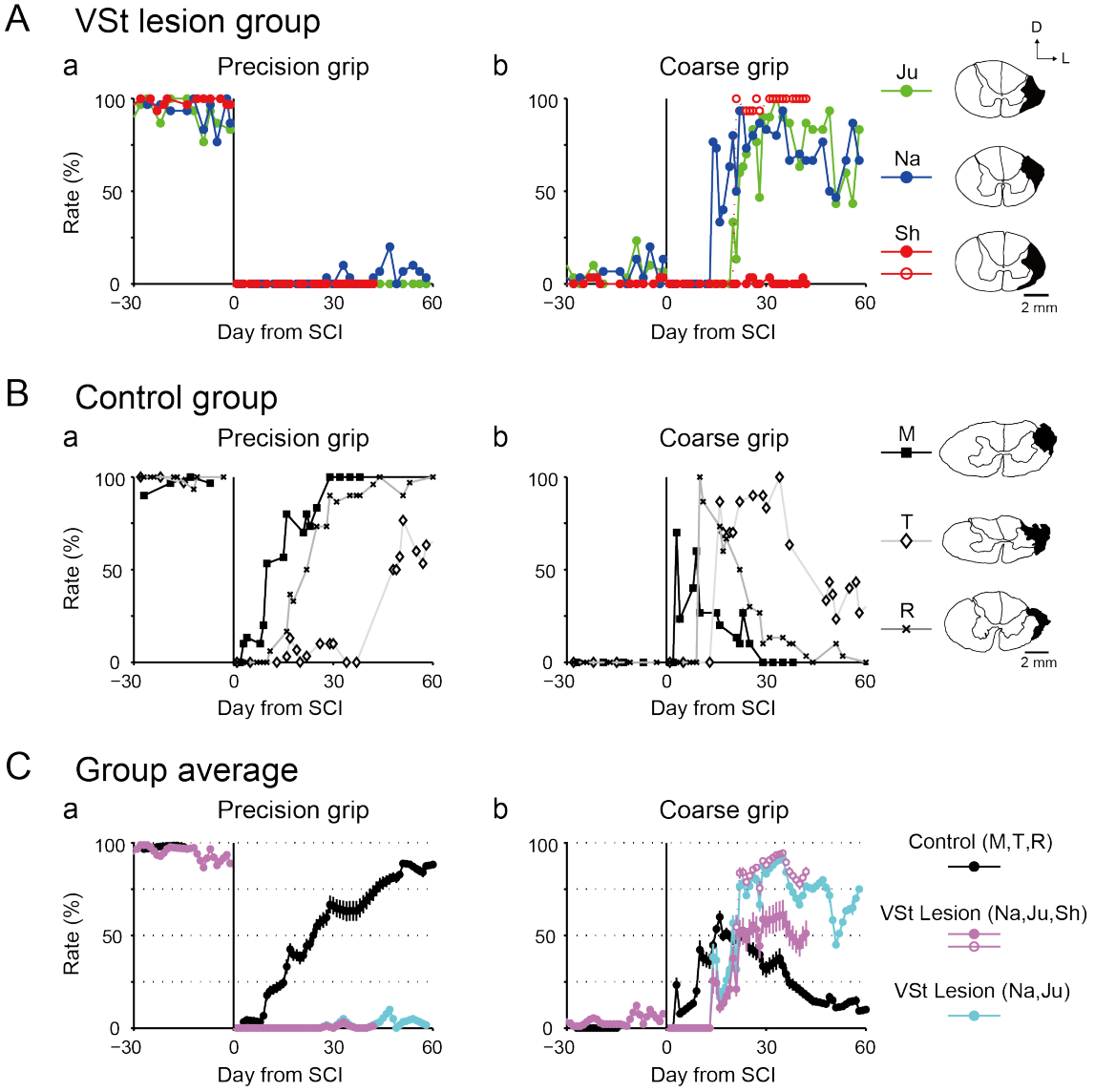

Figure 16: Recovery course of finger movements after SCI. (a) and (b) on (**A**) - (**C**) shows recovery course of the precision grip and the coarse grip, respectively. (**A**): VSt lesion group. Red open circles in (Ab) showed percentage of retrieving with a coarse grip including grasping the dropped food. Since Monkey Sh showed the different strategy

which did not satisfy my criteria of the coarse grip (see Result) (Red filled circles). (**B**): Control group. Recovery course of precision grip in (Ba) was modified from the previous study (Sawada *et al*., 2015). Illustrations of coronal spinal cord sections on right column in (**A**) and (**B**) indicate lesion extent (black hatch) of the l-CST in individual monkeys. D, dorsal; L, lateral. (**C**): Group average. The rate in days was linearly interpolated between recording days for each monkey, and the average rate was calculated in each group. Because of recording days were limited in monkey Sh, two average lines in the VSt lesion group were shown. Data in magenta line obtained from all three monkeys including Monkey Sh. Data in cyan line obtained from two monkeys without Monkey Sh. Because of different strategy in a coarse grip of Monkey Sh [shown by open circles in (Ab)], an additional average line in the VSt lesion group was shown in (Cb). Magenta open circles showed average rate of the coarse grip including the results of two monkeys (Ju and Na) and the result of monkey Sh [red open circles in (Ab)]. Error bars indicate SEM (standard error of the mean) on each day.

General discussion

Motivation is empirically thought to be a critical issue for boosting motor performance, but little is known about the neural mechanism underlying such psychological effects on motor outputs and/or functional recovery after neural damage. Thus, the goal of this thesis was set to uncover the functional role of the mesolimbic system consisting of the VM and VSt, which is commonly thought to be involved in processing motivation (Salamone and Correa, 2013; Floresco, 2015), in facilitation of motor outputs and functional recovery.

In Part I, using non-human primates I investigated the functional pathway from the VM as a part of the mesolimbic system to the spinal cord, by which the VM facilitated outputs to muscles via the M1. This VM–M1–spinal pathway might be a candidate for the neural substrate underlying motivational control of motor outputs. Together with my finding and previous findings showing the VM activation is related to processing motivation (Matsumoto and Hikosaka, 2009) or reward expectation (Schultz *et al*., 1997, 1998), the VM might be a modulatory source of both boosting motivation and enhancing motor outputs simultaneously. In sports that crucially depend on maximum motor output,

such as weightlifting, not only up-regulation of mental state but also simultaneous muscle activations are required. Fast signals to the M1 driven by the VM activation that I found might contribute to such an instantaneous force production via the VM–M1–spinal pathway.

In Part II, I showed the causal contribution of the VSt in functional recovery of the demanding dexterous finger movement after SCI. The VSt has also been implicated as a "reward/pleasure" center and is known to play a critical role in motivational processes. However, recent reviews suggested that the VSt is involved in a rather specific and complex way that cannot be simply explained by the word "reward" (Salamone and Correa, 2012; Floresco, 2015). My results also showed that the VSt was involved in motor control in a specific situation (i.e. after SCI) and during a highly demanding movement. It is likely that the VSt would be critical for regulation of brain activity to overcome demanding situation rather than regulation of simple motivation. Because the VSt–motor-related network was associated with motor control of highly demanding dexterous finger movement after SCI. Together with my findings and classical view of the VSt function, I suggest that the VSt regulates not only motivational processing to take action but also the

activity of motor-related areas, especially when higher effort is required.

Up to today, many scientists have clarified the involvement of the mesolimbic system in motivated behaviors. However, the neural mechanism how the mesolimbic system drives or regulates motor outputs had been unclear. From results of Part I and II, I demonstrated the functional role of the mesolimbic system in motor control and the neural substrate bridging the mesolimbic system and the motor network. Together with classical interpretation of the mesolimbic system as a motivation-/reward-center, I propose that the mesolimbic system can be a critical node which can regulate both motivation and motor outputs simultaneously. My findings might be scientific evidences giving an explanation for suggestions, “psyching-up” (Tod *et al.*, 2003) and “mental energy” (Brodal, 1973) are required for motor outputs in demanding situations.

References (alphabetical order)

1. Aberman JE, Salamone JD. Nucleus accumbens dopamine depletions make rats more sensitive to high ration requirements but do not impair primary food reinforcement. Neurosci 1999; 92: 545-52.

2. Alexander GE, DeLong MR, Strick PL. Parallel organization of functionally segregated circuits linking basal ganglia and cortex. [Review]. Annu Rev Neurosci 1983; 9: 357-81.

3. Arsenault JT, Rima S, Stemmann H, Vanduffel W. Role of the primate ventral tegmental area in reinforcement and motivation. Curr Biol 2014; 24: 1347-53.

4. Belhaj-saif A, Karrer JH, Cheney PD. Distribution and characteristic of poststimulus effects in proximal and distal forelimb muscles from red nucleus in the monkey. J Neurophyiol 1998; 79: 1777-89.

5. Biernaskie J, Chernenko G, Corbett D. Efficacy of rehabilitative experience declines with time after focal ischemic brain injury. J Neurosci 2004; 24: 1245-54.

6. Bortoff GA, Strick PL. Corticospinal terminations in two new-world primates: further evidence that corticomotoneuronal connections provide part of the neural

substrate for manual dexterity. J Neurosci 1993; 13: 5105-18.

7. Brodal A. Self-observations and neuro-anatomical considerations after a stroke. Brain 1973; 96: 675-94.

8. Chemerinski E, Robbinson RG, Kosier JT. Improved recovery in activities of daily living associated with remission of poststroke depression. Stroke 2001; 32:113-7

9. Cheney PD, Mewes K, Widener G. Effects on wrist and digit muscle activity from microstimuli applied at the sites of rubromotoneuronal cells in primates. J Neurophyiol 1991; 66: 1978-92.

10. Chong TT, Bonnelle V, Manohar S, Veromann KR, Muhammed K, Tofaris GK, *et al*. Dopamine enhances willingness to exert effort for reward in Parkinson's disease. Cortex 2015; 69: 40-6.

11. Chiken S, Hatanaka N, Tokuno H. Distribution of median, ulnar and radial motoneurons in the monkey spinal cord: a retrograde triple-labeling study. Neurosci Lett 2001; 307: 143-46.

12. Cléry-Melin ML, Schmidt L, Lafargue G, Baup N, Fossati P, Pessiglione M. Why don't you try harder? An investigation of effort production in major depression.

PLOS ONE 2011; 6: e23178.

13. Descarries L, Lemay B, Doucet G, Berger B. Regional and laminar density of the dopamine innervation in adult rat cerebral cortex. Neuroscience 1987; 21: 807-24.

14. Elliot TR, Frank RG. Depression following spinal cord injury. [Review]. Arch Phys Med Rehabil 1996; 77: 816-23.

15. Fetz EE, Cheney PD. Postspike facilitation of forelimb muscle activity by primate corticomotoneuronal cells. J Neurophysiol 1980; 44: 751-72.

16. Floresco SB. The nucleus accumbens: An Interface between cognition, emotion, and action. [Review]. Annu Rev Psychol 2015; 66:25-52.

17. Frankle WG, Laruelle M, Haber SN. Prefrontal cortical projections to the midbrain in primates: evidence for a sparse connection. Neuropsychopharmacology 2006; 31: 1627-36.

18. Gasper P, Stepniewaks I, Kaas JH. Topography and collateralization of the dopaminergic projections to motor and lateral prefrontal cortex in owl monkeys. J Comp Neurol 1992; 325: 1-21.

19. Haber SN. The primate basal ganglia: parallel and integrative networks. [Review]. J

Chem Neuroanat 2003; 26: 317-30.

20. Haber SN, Fudge JL, McFarland NR. Striatonigrostriatal pathways in primates form an ascending spiral from the shell to the dorsolateral striatum. J Neurosci 20; 2000: 2369-82.

21. Haber SN, Knutson B. The reward circuit: linking primate anatomy and human imaging. [Review]. Neuropsychopharmacology 2010; 35: 4-26.

22. Haber SN, Kunishio K, Mizobuchi M, Lynd-Balta E. The orbital and medial prefrontal circuit through the primate basal ganglia. J Neuroscie 1995; 15: 4851-67.

23. Haber SN, Lynd E, Klein C, Groenewegen, HJ. Topographic organization of the ventral striatal efferent projections in the rhesus monkey: an anterograde tracing study. J Comp Neurol 1990; 293: 282-98.

24. He SQ, Dum RP, Strick PL. Topographic organization of corticospinal projections from the frontal lobe: motor areas on the lateral surface of the hemisphere. J Neurosci 1993; 13: 952-80.

25. Higo N, Nishimura Y, Murata Y, Oishi T, Yoshino-Saito K, Takahashi M, *et al*. Increased expression of the growth-associated protein 43 gene in the sensorimotor

cortex of the macaque monkey after lesioning the lateral corticospinal tract. J Comp Neurol 2009; 516: 493-506.

26. Hosp JA, Pekanovic A, Rioult-Pedotti MS, Luft AR. Dopamine projections from midbrain to primary cortex mediate motor skill learning. J Neurosci 2011; 31:2481-87.

27. Ishida H, Inoue K, Takada M, Hoshi E. Origins of multisynaptic projections from the basal ganglia to the forelimb region of the ventral premotor cortex in macaque monkeys. Eur J Neurosci 2016; 43: 258-69.

28. Jenny AB, Inukai J. Principles of motor organization of the monkey cervical spinal cord. J Neurosci 1983; 3: 567-75.

29. Kapogiannis D, Campion P, Grafman J, Wassermann EM. Reward-related activity in the human motor cortex. Eur J Neurosci 2008; 27:1836-42.

30. Kelly RM, Strick PL. Rabies as a transneuronal tracer of circuits in the central nervous system. J Neurosci Methods 2000; 103: 63-71.

31. Kelly RM, Strick PL. Cerebellar loops with motor cortex and prefrontal cortex of a nonhuman primate. J Neurosci 2003; 23: 8432-44.

32. Kelly RM, Strick PL. Macro-architecture of basal ganglia loops with the cerebral cortex: use of rabies virus to reveal multisynaptic circuits. [Review]. Prog Brain Res 2004; 143: 449-59.

33. Kunori N, Kajiwara R, Takashima I. Voltage-sensitive dye imaging of primary motor cortex produced by the ventral tegmental area stimulation. J Neuorosci 2014; 34: 8894-903.

34. Lacroix S, Havton LA, McKay H, Yang H, Brant A, Roberts J, et al. Bilateral corticospinal projections arise from each motor cortex in the macaque monkey: a quantitative study. J Comp Neurol 2004; 473: 147-61.

35. Lavin A, Nogueira L, Lapish CC, Wightman RM, Phillips PEM, Seamans JK. Mesocortical dopamine neurons operate in distinct temporal domains usinf multimodal signaling. J Neurosci 2005; 25: 5013-23.

36. Lawrence DG, Kuypers HGJM. The functional organization of the motor system in the monkey. I. The effect of bilateral pyramidal lesions. Brain 1968; 91: 1-14.

37. Lewis DA, Cambell MJ, Foote SL, Goldstein M, Morrison JH. The Distribution of tyrosine hydroxylase-immunoreactive fibers in primate neocortex is widespread but

regionally specific. J Neuroscie 1987; 7: 279-90.

38. Luppino G, Matelli M, Camarda R, Rizzolatti G. Corticocortical connections of area F3 (SMA-proper) and are F6 (pre-SMA) in the macaque monkey. J Comp Neurol 1993; 338: 114-40.

39. Marsh BT, Tarigoppula VSA, Chen C, Francis JT. Toward an autonomous brain machine interface: integrating sensorimotor reward modulation and reinforcement learning. J Neuroscie 2015; 35: 7374-87.

40. Matsumoto M, Hikosaka O. Two types of dopamine neuron distinctly convey positive and negative motivational signals. Nature 2009; 459: 837-41.

41. Miyachi S, Lu X, Inoue S, Iwasaki T, Koike S, Nambu A, et al. Organization of multisynaptic inputs from prefrontal cortex to primary motor cortex as revealed by retrograde transneuronal transport of rabies virus. J Neurosci 2005; 25: 2547-56.

42. Mogenson GJ, Jones DL, Yim CY. From motivation to action: functional interface between the limbic system and the motor system. [Review]. Prog Neurobiol 1980; 14; 69-97.

43. Morris PL, Robbinson RG, Raphael B. Prevalence and course of depressive

disorders in hospitalized stroke patients. Int J Psychiatry Med 1990; 20: 349-64.

44. Muir RB, Lemon RN. Corticospinal neurons with a special role in precision grip. Brain Res 1983; 261: 312-6.

45. Murata Y, Higo N, Oishi T, Yamashita Y, Matsuda K, Hayashi M, *et al*. Effects of motor training on the recovery of manual dexterity after primary motor cortex lesion in macaque monkeys. J Neurophysiol 2008; 99: 773-86.

46. Nishimura Y, Morichika Y, Isa T. A subcortical oscillatory network contributes to recovery of hand dexterity after spinal cord injury. Brain 2009; 132: 709-21.

47. Nishimura Y, Onoe H, Morichika Y, Perfiliev S, Tsukada H, IsaT. Time-dependent central compensatory mechanism of finger dexterity after spinal cord injury. Science 2007a; 318: 1150-5.

48. Nishimura Y, Onoe H, Morichika Y, Tsukada H, IsaT. Activation of parieto-frontal stream during reaching and grasping studied by positron emission tomography in monkeys. Neurosci Res 2007b; 59: 243-50.

49. Nishimura Y, Onoe H, Onoe K, Morichika Y, Tsukada H, Isa T. Neural substrates for the motivational regulation of motor recovery after spinal-cord injury. PLOS ONE

2011; 6: e24854.

50. Nudo RJ, Milliken GW, Jenkins WM, Merzenich MM. Use-dependent alterations of movement representations in primary motor cortex of adult squirrel monkeys. J Neurosci 1996; 16: 785-807.

51. Park MC, Belhaj-saif A, Cheney PD. Properties of primary motor cortex output to forelimb muscles in rhesus macaques. J Neurophysiol 2004; 92: 2968-84.

52. Paxinos G, Huang XF, Petrides M, Toga AW. The rhesus monkey brain in stereotaxic coordinates: second edition. London: Academic Press; 2009

53. Perlmutter SI, Maier MA, Fetz EE. Activity of spinal interneurons and their effects on forearm muscles during voluntary wrist movements in the monkey. J Neurophysiol 1998; 80: 2475-94.

54. Pessiglione M, Schmidt L, Draganski B, Kalisch R, Lau H, Dolan RJ, *et al*. How to the brain translates money into Force: a neuroimaging study of subliminal motivation. Science 2007; 316: 904-6.

55. Rathelot J-A, Strick PL. 2006. Muscle representation in the macaque motor cortex: An anatomical perspective. Proc Natl Acad Sci USA 2006; 103: 8257-62.

56. Richard JM, Ambroggi F, Janak PH, Fields HL. Ventral pallidum neurons encode incentive value and promote cue-elicied instrumental actions. Neuron 2016; 90: 1-23.

57. Rosenzweig ES, Brock JH, Culbertson MD, Lu P, Moseanko R, Edgerton VR, *et al.* Extensive spinal decussation and bilateral termination of cervical corticospinal projections in rhesus monkeys. J Comp Neurol 2009; 513: 151-63.

58. Salamone JD, Correa M. The mysterious motivation functions of mesolimbic dopamine. [Review]. Neuron 2012; 76: 470-85.

59. Salamone JD, Yohn SE, López-CrusL, Miguel NS, Correra M. Activational and effort-related aspects of motivation: neural mechanisms and implications for psychopathology. [Review]. Brain 2016; 139: 1325-47.

60. Sasaki S, Isa T, Pettersson LG, Alstermark B, Naito K, Yoshimura K, Seki K, Ohki Y. Dexterous finger movements in primate without monosynaptic corticomotoneuronal excitation. J Neurophysiol 2004; 92: 3142-7.

61. Sawada M, Kato K, Kunieda T, Mikuni N, Miyamoto S, Onoe H, Isa T, Nishimura Y. Function of the nucleus accumbens in motor control during recovery after spinal

cord injury. Science 2015; 350: 98-101.

62. Saxena SK, Ng TP, Koh G, Yong D, Fong NP. Is improvement in impaired cognition and depressive sysmptoms in post-stroke patients associated with recovery in activities of daily living? Acta Neurol Scand 2007; 115; 339-46.

63. Schmidt L, Cléry-Melin ML, Lafargue G, Valabrègue R, Fossati P, Dubois B, *et al*. Get aroused and be stronger: emotional facilitation of physical effort in the human brain. J Neuroscie 2009; 29: 9450-7.

64. Schmidt L, Lebreton M, Cléry-Melin ML, Daunizeau J, Pessiglione. Neural mechanisms underlying motivation of mental versus physical effort. PLOS Biol 2012; 10: e1001266.

65. Schultz W, Dayan P, Montague PR. A neural substrate of prediction and reward. Science 1997; 275: 1593-9.

66. Schultz W. Predictive reward signal of dopamine neurons. [Review]. J Neurophysiol 1998; 80:1-27.

67. Shin JC, Goo HR, Yu SJ, Yoon SY. Depression and quality of life in patients within the first 6 months after the spinal cord injury. Ann Rehabil Med 2012; 36: 119-25.

68. Smith KS, Tindell AJ, Aldridge JW, Berridge KC. Ventral pallidum roles in reward and motivation. [Review]. Behav Brain Res 2009; 196: 155-67.

69. Sugiyama Y, Higo H, Yoshino-Saito K, Murata Y, Nishimura Y, Oishi T, Isa T. Effects of early versus late rehabilitative training on manual dexterity after corticospinal tract lesion in macaque monkeys. J Neurophysiolo 2013; 109: 2853-65.

70. Tachibana Y, Hikosaka O. The primate ventral pallidum encodes expected reward value and regulate motor action. Neuron 2012; 76: 826-37.

71. Thabit MN, Bakatsuka M, Koganemaru S, Fawi G, Fukuyama H, Mima T. Monetary reward induce changes in excitability of primary motor cortex. Clin Neurophysiol 2011; 122:1764-70.

72. Tod D, Iredale F, Gill N. 'Psyching-up' and muscular force production. [Review]. Sports Med 2003; 33:47-58.

73. Tohyama T, Kinoshita M, Kobayashi K, Isa K, Watanabe D, Kobayashi K, *et al.* Contribution of propriospinal neurons to recovery of hand dexterity after corticospinal tract lesions in monkeys. Proc Natl Acad Sci USA 2017; 114: 604-09.

74. Ugolini G. Specificity of rabies virus as a transneuronal tracer of motor networks: transfer from hypoglossal motoneurons to connected second-order and higher order central nervous system cell groups. J Comp Neurol 1995; 356: 457-80.

75. Watanabe Y, Kajiwara R, Takashima I. Optical imaging of rat pre- frontal neuronal activity evoked by stimulation of the ventral tegmental area. Neuroreport 2009; 20: 875– 880.

76. Widener GL, Cheney PD. Effects on muscle activity from microstimuli applied to somatosensory and motor cortex during voluntary movement in the monkey. J Neurophysiolo 1997; 77: 2446-65.

77. Williams S, Goldman-Rackic PS. Widespread origin of the primate mesofrontal dopamine system. Cereb Cortex 1998; 8: 321-45.

78. Winchester P, McColl R, Querry R, Foreman N, Mosby J, Tansey K, *et al*. Changes in supraspinal activation patterns following robotic locomotor therapy in motor-incomplete spinal cord injury. Neurorehab Neural Repair 2005; 19: 313-24.

79. Yoshino-Saito K, Nishimura Y, Oishi T, Isa T. Quantative inter-segmental and inter-laminar comparison of corticospinal projections from the forelimb area of the

primary motor cortex of macaque monkeys. Neuroscience 2010; 171: 1164-79.

Acknowledgements

The dissertation is a part of the requirements for receiving the doctor's degree, conferred by SOKENDAI. First, I would like to express my deepest gratitude to my supervisors, Dr. Yukio Nishimura (Neural Prosthesis Project, Tokyo Metropolitan Institute of Medical Science) and Prof. Tadashi Isa (Department of Neuroscience, Graduate School of Medicine, Kyoto University) for their critical discussions and encouragements for this research. I would also like to appreciate Prof. Masaki Isoda [Department of System Neuroscience, the National Institute for Physiological Sciences (NIPS)] for his encouragement for this research. Major part of the studies was conducted in NIPS. I would also like to thank Nobuaki Takahashi and Yumi Yamanishi in NIPS, for their assistance in training monkeys, surgeries and experiments. I would never have succeeded in running my experiments without their assistance.

I also thank Profs. Masahiko Takada, Ken-ichi Inoue and Dr. Hiroshi Nakagawa in the Systems Neuroscience Section, Primate Research Institute, Kyoto University, for their help in the anatomical experiment using retrograde trans-synaptic tracer, rabies virus, and also their advice on this research. I also have appreciated Kayo Onoe and Hirotaka

Onoe in Bio-Function Imaging Team, RIKEN Center for Life Science Technologies for their instruction and help in analysis of the PET experiment. Dr. Hirotaka Onoe gave me great advices and improved discussion and interpretation relating to the SCI experiment. I would also like to thank Drs. Noriyuki Higo and Yumi Murata in Systems Neuroscience Group, National Institute of Advanced Industrial Science and Technology, for their help to identify the lesion areas induced by ibotenic acid injection.

Finally, I would like to thank my parents and all other members of Isa laboratory in NIPS and Kyoto University; Masatoshi Yoshida, Masaaki Ogawa, Zenas Chao, Hidenori Watanabe, Rikako Kato, Masatoshi Kasai, Shusaku Sasada, Kenji Kato, Richard Veale, Denis Matrov, Norihiro Takakuwa, Seiya Ishino, Yoko Nishihara, Yaoki Nakao, Kota Tokuoka, Griffin St. Clair, Yusuke Yamamoto, Masahiro Sawada, Takamichi Tohyama, Morio Togawa, Kaoru Isa, Kotomi Shimizu, Toshie kuwahara, Kazuko Takada, Shoko Yamazaki, Maasa Ishino, Ayumi Shibata, Yu Shimada, Jiro Yamashita and Erina Morie for the encouragement for this research.